



This is to certify that the

thesis entitled

EPR Studies Of Cs+(1886)(1505)e-And Li+(C211)e-

presented by

Kerry Ann Reidy

has been accepted towards fulfillment of the requirements for

Masters __degree in __ Chemistry

Major professor

Date July 30, 1992

O-7639

MSU is an Affirmative Action/Equal Opportunity Institution

LIBRARY Michigan State University

PLACE IN RETURN BOX to remove this checkout from your record. TO AVOID FINES return on or before date due.

DATE DUE	DATE DUE	DATE DUE

MSU is An Affirmative Action/Equal Opportunity Institution

		'
		! ;
		:
		:

EPR STUDIES OF Cs⁺(18C6)(15C5)e⁻ AND Li⁺(C211)e⁻

By

Kerry Ann Reidy

A THESIS

Submitted to
Michigan State University
in partial fulfillment of the requirements
for the degree of

MASTER OF SCIENCE

Department of Chemistry

ABSTRACT

EPR STUDIES OF Cs+(18C6)(15C5)e-AND Li+(C211)e-

By

Kerry Ann Reidy

The similarities between Cs+(18C6)₂e-, Cs+(15C5)₂e-, and Cs+(18C6)(15C5)e-, have been explored via electron paramagnetic resonance techniques. It was found that the mixed sandwich compound yielded different EPR results than the two "parent" compounds. The number of paramagnetic centers changed throughout the temperature range of about 100-200 K in the mixed sandwich compound, thus disobeying the Curie Law in that temperature range. The number of unpaired spins remained the same in the two "parent" compounds within that same temperature range, thus they followed the Curie Law. This finding suggests that the mixed sandwich compound does not behave merely as a mixture of the two "parent" compounds, but as a unique compound.

Similar EPR studies of Li⁺(C211)e⁻ revealed very inconsistent results. This compound has traditionally been the most difficult to handle, which contributes to the inconsistencies observed from the EPR results.

ACKNOWLEDGMENTS

I would first like to thank the two research advisors who have supervised me and guided me over the last two years, Dr. John McCracken and Dr. James Dye. Their ultimate wisdom and enthusiasm was the driving force for this research and I am grateful to the both of them. I only hope that I can live up to their expectations over the next three years. I thank the two research groups with whom I have worked, in particular Hong-In Lee for the many helpful quantum mechanical discussions and especially to Michelle Mac for experiencing this ordeal with me and always lending a helping hand.

I thank my family and friends for being patient with me and for being understanding. Without them, I may not have made it this far.

Lastly, I thank Robert Cedergren for the many sleepless nights helping me with this document, for listening to me, for putting up with me during the crucial last minute, and for all of his love and support over the past two years.

K.A.R.

TABLE OF CONTENTS

Page
LIST OF TABLESiv
LIST OF FIGURESv
CHAPTER 1.
Historical Background of Alkalides and electrides1
CHAPTER 2.
Experimental Procedures for the Synthesis of
Cs+(18C6)(15C5)e18
CHAPTER 3.
Theoretical Approach to Electron Paramagnetic
Resonance27
CHAPTER 4.
EPR Results and Discussion of Cs+(18C6)(15C5)e-
and Li ⁺ (C211)e ⁻ 39
CHAPTER 5.
In the Future
I. Advanced EPR Studies of some HMHCY Sodides53
II. EPR Studies of the Photoexcited Triplet State of
K+(C222)e- and K+(C222)K62
III. Synthesis and Characterization of New Alkalides
and Electrides64

REFERENCES	66
APPENDIX	69

LIST OF TABLES

		Page
1.	Structural data for alkalides and electrides	6
2.	EPR results for one of three samples of Cs+(18C6)(15C5)e	42
3.	Comparison of Cs ⁺ (18C6) ₂ e ⁻ , Cs ⁺ (15C5) ₂ e ⁻ and	
	Cs+(18C6)(15C5)e	48

LIST OF FIGURES

	Pa	ge
1.	Typical complexants used to synthesize alkalides and	
	electrides	3
2.	F-center, a negative ion vacancy with one excess electron bound at	
	the vacancy	7
3.	Interstitial ion or Fraenkel defect	8
4.	Representation of the ion packing in Cs+(18C6) ₂ Na ⁻ (top) and	
	Cs+(HMHCY)Na- (bottom)	11
5.	Magnetic susceptibility data $[1/\chi_e^m \text{ vs. } T(K)]$ for Cs ⁺ (15C5) ₂ e ⁻	.14
6.	Common organic solvents. The 1° and 2° amines are not as	
	resistive to reduction as the ethers or the 3° amines due to the	
	ionizable protons on the former amines	19
7.	K-cell used in the synthesis of alkalides and electrides	.21
8.	Precession of electron spin angular momentum and magnetic	
	moment in a magnetic field	.28
9.	Electron spin levels in a magnetic field. Resonance is achieved	
	when the frequency of the incident radiation matches the frequency	
	corresponding to the energy level separation	.30
10	. Energy level diagram describing the effect of nuclear hyperfine	
	interaction	36
11	. Schematic diagram of a CW-EPR spectrometer	38

12.	CW-EPR spectra of Cs ⁺ (18C6)(15C5)e ⁻ at temperatures of 91K	
	(top spectrum) and 221K (bottom spectrum)	40
13.	Relative intensity vs. reciprocal temperature (1/K) for	
	Cs+(18C6)(15C5)e	43
14.	Asymmetry of lineshape with respect to inverse lineshape	46
15.	CW-EPR spectra of Li ⁺ (C211)e ⁻ at temperatures of 90K	
	(top spectrum) and 220K (bottom spectrum)	50
16.	Intensity vs. 1/T from EPR results of Li+(C211)e	51
17.	Individual spin packets which are homogeneously broadened	
	enveloped by an inhomogeneously broadened line	55
18.	Evolution of the magnetization during a single $\pi/2$ pulse	56
19.	2-pulse echo sequence and evolution of the magnetization	58
20.	Allowed and semi-forbidden transitions in an EPR spectrum	59
21.	Echo diagram describing echo nuclear modulation a) after $\pi/2$	
	pulse, b) after π pulse, c) at the time of the echo	61
22.	CW-EPR spectrum of K+(C222)K- at 130 K	63
23.	Two aromatic complexants used to produce potential alkalides	
	and electrides	65

CHAPTER 1

HISTORICAL BACKGROUND OF ALKALIDES AND ELECTRIDES

The group IA elements, or alkali metals, most commonly take on the plus one oxidation state. In fact, they are so reactive in their metallic form that this form does not exist in nature. It has traditionally been taught in freshman chemistry classes that these metals will eagerly give up an electron to form a stable salt, such as sodium chloride. This occurs in part due to the fact that both sodium and chloride now take on a more stable inert gas electron configuration. Adding an electron to an alkali metal fills the s-orbital but in a less strongly favored configuration then the inert gas configuration, so it was deemed *highly* unlikely. In the year 1974, it was found that alkali metals, under very specific conditions, could form stable salts where the alkali metal maintains both a plus one oxidation state as well as the peculiar minus one oxidation state ^{1a-d}. The research group of Dr. James L. Dye discovered these crystalline salts and the research still continues today.

These crystalline compounds consist of an alkali metal cation encapsulated by some complexant along with some anion, either an alkali metal anion or an electron. These materials represent new classes of compounds coined alkalides and electrides. The main difference between the two compounds is the anion. In alkalides, an alkali metal is the anion

while in electrides, an electron is the anion. Electrides originate from solvated electrons and alkalides from solvated alkali metal anions. Solvated electrons are thought of as electrons in solution that do not belong specifically to one single molecule or even to a collection of molecules which maintain a well defined geometry. They are not trapped as in organic glasses. Because of the light mass of the electrons, they are considerably more mobile than other anions in salts thus they are fairly free to travel throughout the solution which contributes to their unique properties. These properties of solvated electrons have been studied by several different research groups in a time period of over eighty years². It was observed many years ago that if a chunk of sodium was reacted with pure anhydrous ammonia, a deep blue solution formed. This blue solution was thought to indicate the solvated electron. When preparing the stable solutions that contain solvated electrons or alkali metal anions, solvent choice is of high importance. The solvent needs to be resistant to reduction and to be a strong solvator of the cation but the process of solvating the electron or anion is of lower importance. However, alkali metals only dissolve in a few solvents other than ammonia, such as hexamethylphosphoramide (HMPA), a few primary amines, and a few polyethers.

By making use of the discovery of crown ethers by Pederson³ in 1967, and of cryptands (Figure 1) by Jean-Marie Lehn⁴ in 1969, the Dye group showed that the solubility of the alkali metals could be greatly increased. It follows then that an important aspect of synthesizing alkalides or electrides is the complexing ability of the species that complexes the cation. The particular complexant must be resistant to reduction as well as

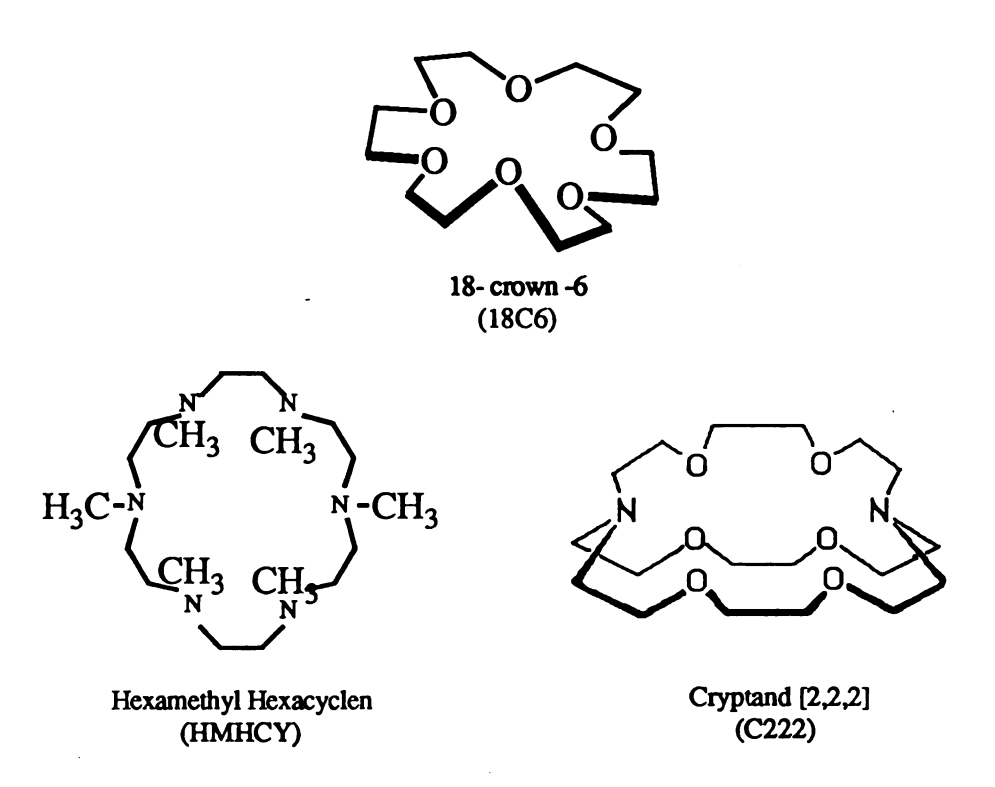


Figure 1: Typical complexants used to synthesize alkalides and electrides

be a strong enough complexant such that it will win the battle for solvating the cation over any strongly polar solvent. These cyclic and bicyclic complexants are nearly resistant to reduction and deprotonation and have been quite useful in the development of alkalide and electride synthesis. The role of the complexant is to encapsulate the alkali metal cation so that the electron that the metal ejects will go into solution, or attach to an alkali metal to form the metal anion in solution.

After proper work-up procedures, eventually the electron will either remain as itself in the solid structure, or add to some remaining unreacted alkali metal to form the alkali metal anion in solution and/or in the solid. To be more specific, 18-crown-6 is a very common complexant used in this research and when the alkali metal, the solvent and the complexant come into contact with one another, the complexant encapsulates the alkali metal cation on the hole formed by the ring. The lone pairs of electrons on the oxygen atoms in the ether unit of the crown, are oriented towards the positive ion, thus providing stability of the complex. The complexants play other roles in the synthesis of alkalides and electrides. For example they play an integral part in aiding in the solvation of the alkali metal in certain solvents that cannot dissolve the metal alone. This increases the list of only a handful of solvents available for use to several more and greatly enhances the solubility. The equilibria of the reactions are shifted:

$$M_{(s)} \longrightarrow M^+ + e_{solv}$$
 (I-1)

$$M^{+} + C \longrightarrow M^{+}C$$
 (I-2)

where C represents the complexant. These equilibria, together with equation I-3,

$$M_{(s)} + e_{solv} \longrightarrow M$$
 (I-3)

allow us to synthesize concentrated alkali metal solutions in solvents such as tetrahydrofuran (THF) or dimethyl ether (Me₂O) that contain M⁺C with the counterion as either M⁻ or the solvated electron, or perhaps a mixture of the two. It is possible to adjust the concentration of the relative anionic species by changing the ratio of complexant to metal. However, some solutions will contain both M⁻ and solvated electrons in addition to some unreacted complexants, even if it is a stoichiometric solution. In the absence of complexant, the solubility of the metal is often very small. When this is true and the cation complexation constant is very large, these two equilibria can be used to describe the behavior, (Eqs. I-4, I-5).

$$M_{(s)} + C \longrightarrow M^{\dagger}C + e_{solv}$$
 (I-4)

$$2M_{(s)} + C \longrightarrow M^{+}C + M^{-}$$
 (I-5)

In preparing the alkalides or electrides, a second solvent that is less polar than the first is added so that the polycrystalline material falls out of solution. If the crystals are of appropriate shapes and sizes, the crystal structure can be attempted. Up to now, the crystal structures have been solved for 30 alkalides and four electrides, (Table 1).

Table 1

Structural Data for Alkalides and Electrides

	 		
Compound	Space Group	Compound	Space Group
Cs+(18C6) ₂ e-	Monoclinic	Rb+(18C6)Rb-	Monoclinic
Cs+(15C5) ₂ e-	Triclinic	Cs+(C222)Cs-	Monoclinic
Li+(C211)Na-	Orthorhombic	K+(HMHCY)Na-	Orthorhombic
Na+(C222)Na-	Rhombohedral	Rb+(HMHCY)Na-	Orthorhombic
Na+(C221)Na-	Monoclinic	Cs+(HMHCY)Na-	Orthorhombic
K+(C222)Na-	Orthorhombic	Rb+(18C6)Na-MeNH ₂	Orthorhombic
K+(12C4) ₂ Na-	Monoclinic	K+(18C6)(12C4)Na-	Orthorhombic
Rb+(15C5) ₂ Na-	Monoclinic	K+(18C6)(12C4)K-	Orthorhombic
Cs+(18C6) ₂ Na-	Monoclinic	K+(18C6)(12C4)K(18C6)	Monoclinic
Cs+(15C5) ₂ Na-	Triclinic	Li+2(TMTCY)2(MeNH)Na-	Orthorhombic
Cs+(15C5) ₂ K-	Triclinic	Li+2(TMTCY)2(MeNH)Na-	Orthorhombic
Rb+(15C5) ₂ Rb-	Monoclinic	Li ⁺ 2(TMTCY)	Orthorhombic
		(DMTCY)-MeNH ₂ Na-	
Cs+(18C6) ₂ Cs-	Orth. Pbca	Li+(18C6)Na-(MeNH ₂) ₂	Monoclinic
Li+(C211)e-	Orth. Pbcn	Li+(18C6)Na-(MeNH ₂) ₂ .(18C6) ₃	Rhombohedral
K+(C222)e-	Monoclinic	Cs+(18C6)(15C5)Na-	P21/m
K+(C222)K-	Triclinic	K+(18C6)Na ⁻ (MeNH ₂) ₂ .(18C6)	Rhombohedral
Rb+(C222)Rb-	Triclinic	Li+(MICH)Na-) ₂ (MeNH ₂)	Monoclinic

A pure alkalide would consist of an alkali metal with an ns° electron configuration (M⁺) and ns² electron configuration (M⁻) (where the metals need not be the same) thus they are expected to be diamagnetic. However, magnetic susceptibility and EPR studies have shown that some paramagnetic species do exist in these polycrystalline materials. The reason for this is due to the presence of trapped electrons in anionic vacancies in the crystals. These defect electrons occupy holes, and such electron-occupied holes are called F-centers (Figure 2).

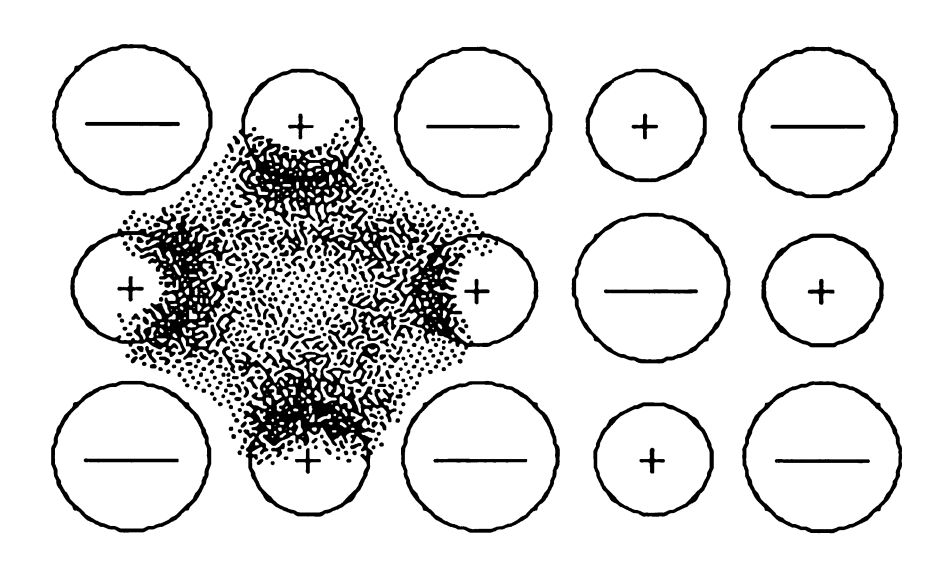


Figure 2: An F-center is a negative ion vacancy with one excess electron bound at the vacancy.

The electron of an F-center can generally be thermally excited to a conduction band⁵, thus giving rise to an n-type semi-conductor. Another type of defect electron that possibly exists in these systems is an interstitial defect or Fraenkel defect (Figure 3). The fact that the electrons are weakly

bound has been taken advantage of in that photoelectron emission and thermionic emission have been demonstrated from alkalides and electrides.

Because of the wide range of behavior of the magnetic properties of electrides and alkalides, as well as the optical and electronic properties, these compounds can act as a probe for determining the interactions of weakly bound electrons with each other and with surrounding ions and molecules.

Electron spin echo envelope modulation (ESEEM) is a pulsed EPR technique that can take on the challenge of mapping these electrons and their interactions. This topic will be addressed in a later chapter.

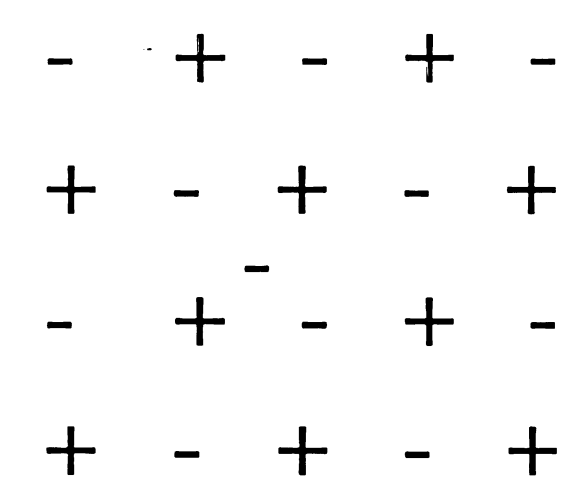


Figure 3: <u>Interstitial Ion (Fraenkel defect)</u>
a distortion in a point because there is an atom in a position where it does not belong.

The most extensively studied alkalide to date is Na+(C222)Na-1b,c, mainly because of its remarkable stability relative to the other alkalides and electrides. Even though most of these ionic salts are sensitive to air, moisture, and to other reducing agents as well as to temperature, Na+(C222)Na- is stable under vacuum for several days at room temperature and indefinitely at low temperature. However it is thermodynamically unstable towards decomposition. Crystalline alkalides and electrides are subject to an irreversible decomposition process as the temperature is raised. The decomposition usually accelerates at around 0°C although this is dependent upon the system. The crystal structure of Na+(C222)Na- has been found to be rhombohedral with a space group in the hexagonal setting.

The Na⁺(C222)Na⁻ crystal is a very brilliant gold-copper color and one might think that it is a metal. However, it is not a metal and instead is an intrinsic semi-conductor with an apparent band gap of 2.4 eV^{1b}. EPR studies as well as magnetic susceptibility studies show that the pure Na⁺(C222)Na⁻ material is only weakly paramagnetic, whether in the form of a powder, thin film or microcrystal. The effect of light was studied by recording the EPR spectrum while the sample was illuminated in the cavity^{1b}. Illumination of the sample was provided by a 150W tungsten lamp which was focused directly on the grid of the EPR cavity. Unfiltered visible light (UV excluded) or 630 nm light, produced an increase in the EPR signal. The results from the EPR measurements showed only the photoproduction of a low concentration of paramagnetic species. The g-value was found to be 2.005 which is close to that of trapped electrons in solids of this type. No other paramagnetic species were observed. The lifetime at room temperature of the paramagnetic species was long, with a

half-life of about 30 seconds. The addition of EPR active material was thought to be due to the dissociation of defect electron pairs which were present before illumination of the Na+(C222)Na-.

Other alkalides and electrides were studied via EPR yielding quite interesting results. In one study⁶, various EPR measurements of sodides were compared. Three of the sodides were sandwich compounds, in which two complexant molecules encapsulate the cation, and three sodides involved the complexant hexamethyl hexacyclen (HMHCY) (see Figure 1). In the sandwich compounds, [Cs+(18C6)₂Na-, Cs+(15C5)₂Na-, Cs+(12C4)₂Na-], each Cs+ ion is sandwiched between pairs of the respective crown ether, while the Na- ion is surrounded by eight such complexed cations, at roughly equal distances. In the other compounds, each HMHCY complexed Cs+, Rb+ or K+ is nearly in contact with Na- at much larger distance from other anionic sites (Figure 4).

The HMHCY sodides provided atypical EPR spectra in that resolved hyperfine splitting existed following the 2nI + 1 rule for a number of EPR lines (where n = the number of identical nuclei involved and I = the nuclear spin). For example, Cs has a spin of I = 7/2 so if the trapped electrons in the anionic site were close enough to the Cs ion to interact, one would expect [2(1)(7/2)+1=8] an eight line pattern. This is in fact what is observed. The same pattern is observed for Rb (I = 5/2), a six line pattern and K (I = 3/2) a four line pattern. A direct measurement of the isotropic part of the hyperfine coupling constant was made from each spectrum.

The behavior of the EPR intensities was also measured as a function of temperature. In general, these systems follow Curie Law behavior. A plot of intensity versus 1/T (K) yielding a straight line follows Curie's Law. Thus the concentration of unpaired spins is constant during that

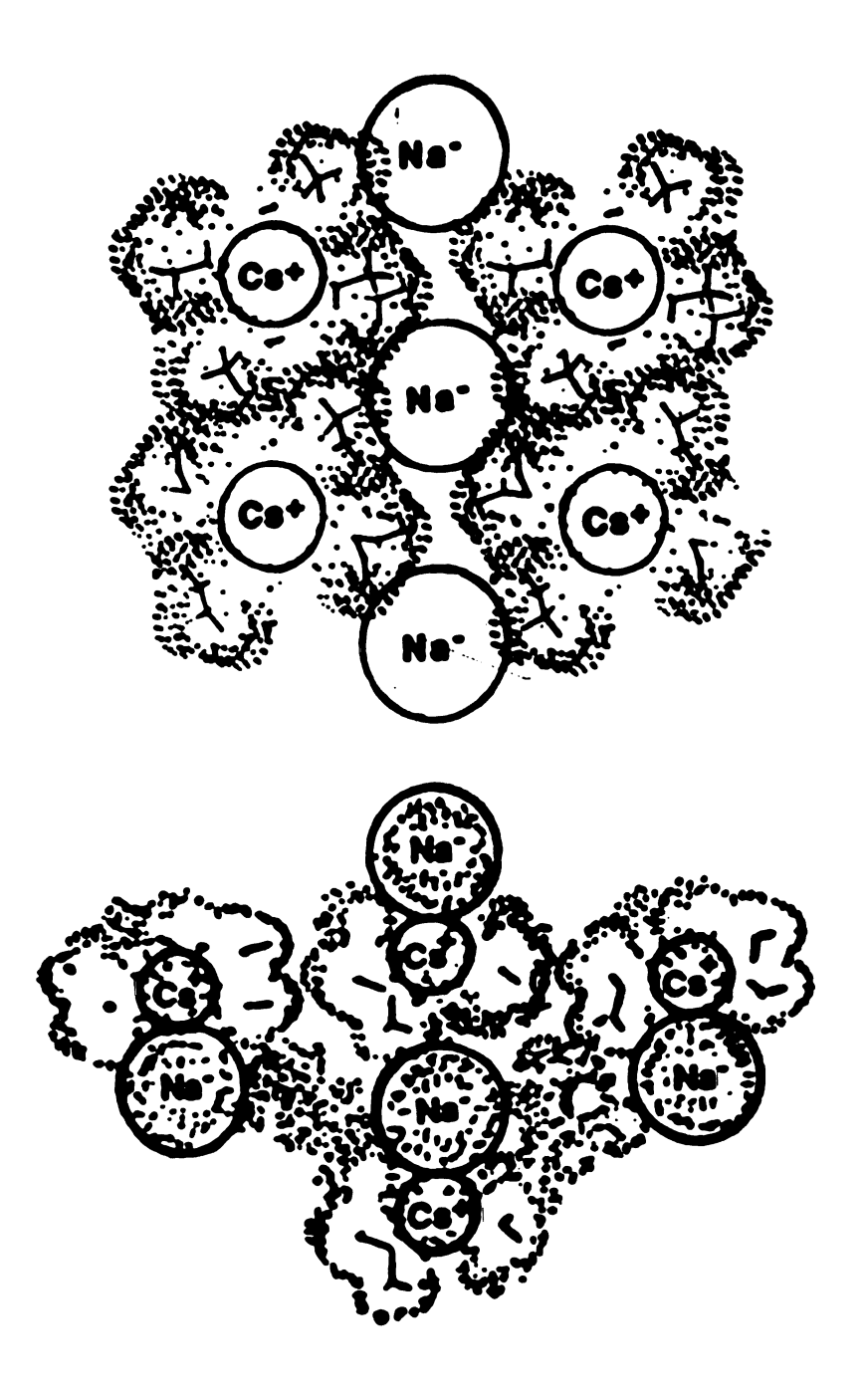


Figure 4: Representation of the ion packing in Cs+(18C6)₂Na- (top) and Cs+(HMHCY)Na- (bottom).

particular temperature range. Furthermore, the trapped electrons do not strongly interact with each other. Interestingly, K+(HMHCY)Na- showed no temperature dependence of the signal intensity during the temperature change of 190 - 240 K. A possible explanation of this is spin pairing or antiferromagnetic coupling between electrons with different temperature dependences in the two sites.

The EPR measurements revealed only a single line for the two sandwich compounds, Cs+(15C5)₂Na- and Cs+(12C4)₂Na- with g-values of 2.0020 and 2.0025, respectively. These are close to the free electron g-value which implies that little spin-orbit coupling exists. The peak to peak line widths were 2.21 and 4.40 G respectively. These spectra provided very little information.

In contrast, the sandwich compound Cs+(18C6)₂Na- showed a broad line with a sharp central narrow line. Each synthesis was slightly different so the relative intensities of the two peaks also varied. The spectrum showed no resolved hyperfine coupling and the line broadening was thought to come from superhyperfine interactions with several surrounding nuclei rather than a shifting of the g-values. The differences in the structures of these two families of compounds clearly agrees with the fact that hyperfine interactions are observed for the contact HMHCY complexes, while none is seen for the sandwich compounds.

What happens when two different types of crown ethers are forced to react under the proper conditions, with an alkali metal? In this case, a mixed sandwich was formed and the properties of these types of compounds are presently being studied. Here I would like to discuss the comparison between Cs+(18C6)₂e-, Cs+(15C5)₂e-, and later, compare these

results with those found in this study of the most recent mixed sandwich compound, Cs+(18C6)(15C5)e⁻.

The crystal structure of Cs+(15C5)₂e⁻ belongs to the triclinic space group in which the electride contains only complexed cations, Cs+(15C5)₂, and trapped electrons that were undetectable by x-ray diffraction⁷. The Cs+-O distances have an average value of 3.154 Å. The apparent band gap of this compound was at least 1.0 eV and it was thought to be an insulator. This system involved localized electrons with a ground state energy at least 1.0 eV below the conduction band, as indicated by the the fact that no detectable intrinsic electronic conductivity was observed below 190K⁸. It was later found that this system was an ionic conductor rather than an electronic conductor with an activation energy of 0.6 eV⁹. These results were sample dependent however.

The magnetic susceptibility of Cs+(15C5)₂e⁻ showed Curie-Weiss behavior⁸ down to 2K after being quenched from room temperature to 5K (Figure 5). However, different behavior was observed when the Cs+(15C5)₂e⁻ was gradually cooled from 250 K. An antiferromagnetic transition occurs with a Neél temperature of 4.2 K. However, at temperatures well above the Neél temperature, the susceptibility followed the Curie-Weiss law. Several NMR experiments were carried out on this electride⁸. Initially, two peaks were observed with chemical shifts at 490 ppm and 290 ppm from a temperature range of 265-280 K. Above 280 K, only one peak was observed at 290 ppm, most likely due to a phase transition at that temperature. EPR measurements¹⁰ revealed a single narrow line for three samples at 200 K. The peak to peak linewidth was 0.6 G with a g-value of 2.0022±1x10⁻⁴. The samples subject for EPR analysis were always quenched from 270K - 2.5K. and followed the 1/T

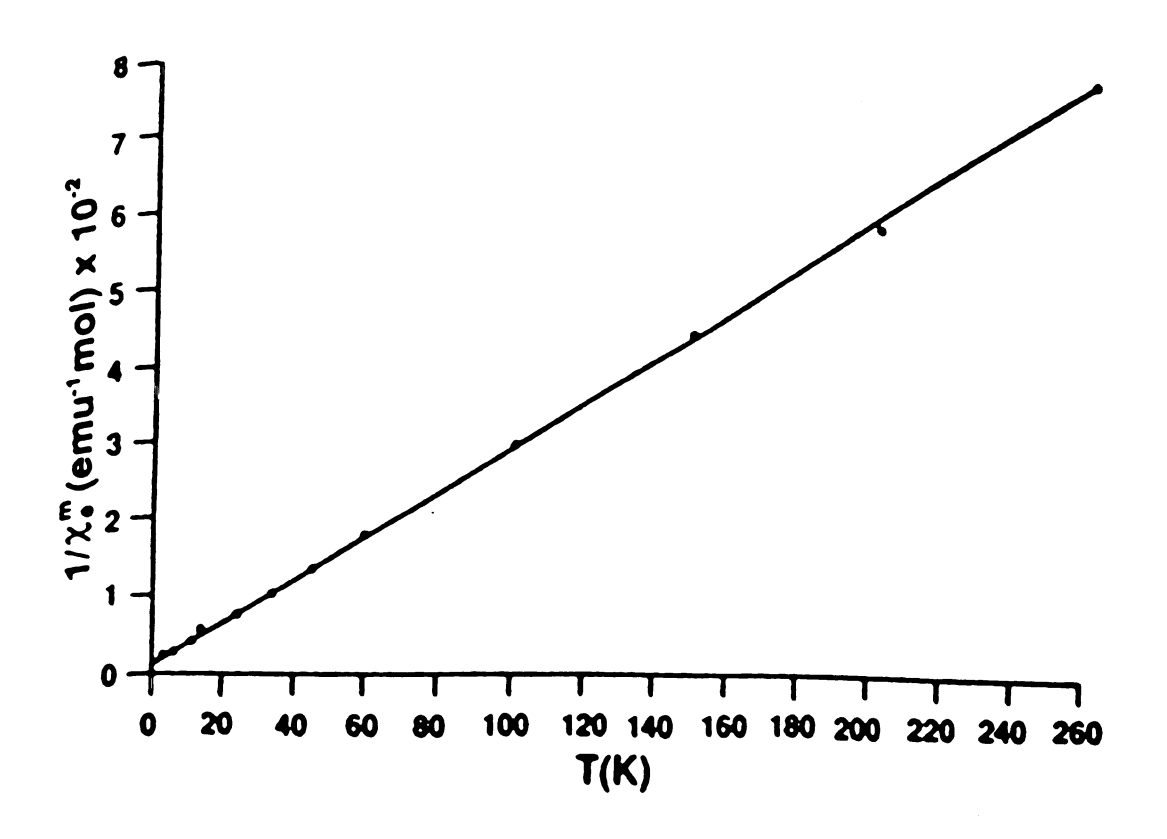


Figure 5: Magnetic susceptibility data (1/Xe^m versus temperature) for Cs+(15C5)₂e⁻.

dependence expected for Curie-Weiss paramagnets. There was no significant shift in the g-value with temperature, but it was found that the peak to peak linewidth increased with decreasing temperature.

Cs⁺(18C6)₂e⁻ was the first electride to have its crystal structure determined, which was found to be monoclinic¹¹. The crystal structure, as well as optical, electrical, and magnetic properties, show that Cs⁺(18C6)₂e⁻ has each electron trapped in an elliptically-shaped empty cavity of a radius about 2.4 Å. In addition, each electron was found to be surrounded by eight sandwich-complexed cesium cations. Initial conductivity studies showed that this compound had an apparent band gap of 0.9 eV. which implied that this electride was a semi-conductor¹². However, later it was shown that this compound indicated the presence of ionic conductivity which is in disagreement with the previous results⁸. ¹³³Cs NMR had been shown to be a primary technique for the characterization of Cs⁺(18C6)₂e⁻ and it was used as a probe to understand the interactions of the trapped electron with the encapsulated cation. The electrons appeared to be localized and were found to interact with each other and the cation only weakly. The NMR results showed only one peak with a chemical shift of +81ppm¹³. This chemical shift describes a paramagnetic shift from that of other Cs(18C6)₂ compounds which could be due to contact with the electron, or perhaps a tighter coordination of the Cs with the crown ethers. The paramagnetic shift in the Cs⁺(18C6)₂e⁻ is the contact shift (or Knight shift). The paramagnetic electron density produces a strong magnetic field at the nucleus which results in the Knight shift. The fact that there was only one NMR peak present in the ¹³³Cs NMR (due only to Cs+ and no Cs-), and that the peak was shifted paramagnetically, was consistent with this compound being an electride.

dependence expected for Curie-Weiss paramagnets. There was no significant shift in the g-value with temperature, but it was found that the peak to peak linewidth increased with decreasing temperature.

Cs⁺(18C6)₂e⁻ was the first electride to have its crystal structure determined, which was found to be monoclinic¹¹. The crystal structure, as well as optical, electrical, and magnetic properties, show that Cs+(18C6)₂ehas each electron trapped in an elliptically-shaped empty cavity of a radius about 2.4 Å. In addition, each electron was found to be surrounded by eight sandwich-complexed cesium cations. Initial conductivity studies showed that this compound had an apparent band gap of 0.9 eV. which implied that this electride was a semi-conductor¹². However, later it was shown that this compound indicated the presence of ionic conductivity which is in disagreement with the previous results⁸. ¹³³Cs NMR had been shown to be a primary technique for the characterization of Cs⁺(18C6)₂e⁻ and it was used as a probe to understand the interactions of the trapped electron with the encapsulated cation. The electrons appeared to be localized and were found to interact with each other and the cation only weakly. The NMR results showed only one peak with a chemical shift of +81ppm¹³. This chemical shift describes a paramagnetic shift from that of other Cs(18C6)₂ compounds which could be due to contact with the electron, or perhaps a tighter coordination of the Cs with the crown ethers. The paramagnetic shift in the Cs⁺(18C6)₂e⁻ is the contact shift (or Knight shift). The paramagnetic electron density produces a strong magnetic field at the nucleus which results in the Knight shift. The fact that there was only one NMR peak present in the ¹³³Cs NMR (due only to Cs⁺ and no Cs⁻), and that the peak was shifted paramagnetically, was consistent with this compound being an electride.

were locally trapped and that they exhibited spin pairing as the temperature was decreased. Finally, crystalline material was synthesized and characterized, and the space group symmetry of the Li+(C211)e- was found to be orthorhombic. Once the crystalline material could be produced, it was found via magnetic susceptibility, that the electride might be independent of the ratio, Li/complexant. In addition, the magnetic susceptibility results showed an anti-ferromagnetic behavior, thus the data could not be fit by the Curie-Weiss equation. EPR results of the new and improved crystalline material should help clear up some of the mysteries of this electride.

EPR studies of the type discussed here are continued in this research, focussing on Cs+(15C5)(18C6)e- and Li+(C211)e-. Clarification of some of the uncertainties with the Li+(C211)e- characteristics as well as a comparison between the mixed sandwich electride, Cs+(18C6)(15C5)e-, and the other two similar electrides, Cs+(18C6)₂e- and Cs+(15C5)₂e- were attempted. It is worthwhile to proceed in the next chapter with a detailed explanation of the experimental procedures.

CHAPTER 2

EXPERIMENTAL PROCEDURES FOR THE SYNTHESIS OF Cs+(18C6)(15C5)e-

Preparation of alkali metal solutions, alkalides and electrides would not be as tedious if the highly reactive nature of the solvated or trapped electron and alkali metal anions did not exist. Oxygen, water, alcohols and other reducible substances must be kept out of the reaction vessel. Furthermore, the reaction vessel must be immersed in a cold bath at temperatures around -40°C during synthesis and kept cold during use and storage of the alkalides and electrides. Presumably, the reason for this is that the complexants and solvents are themselves reducible substances 16. This ultimately leads to decomposition of the solid or solution. A solvent such as dimethyl ether is a preferred solvent because of its resistance to reduction. Since dimethyl ether (Me₂O) does not have ionizable protons, or protons that are beta to the oxygen, this leads to resistance to reduction, so that it is a very robust solvent. Primary and secondary amines have ionizable protons, thus making them less desirable. Trimethylamine (TMA) and, to some extent, diethyl ether (Et₂O) also maintain a resistance towards reduction, although Et₂O has beta hydrogens, and these two solvents serve as suitable co-solvents (Figure 6). The combination of Me₂O and TMA provides the greatest resistance to reduction.

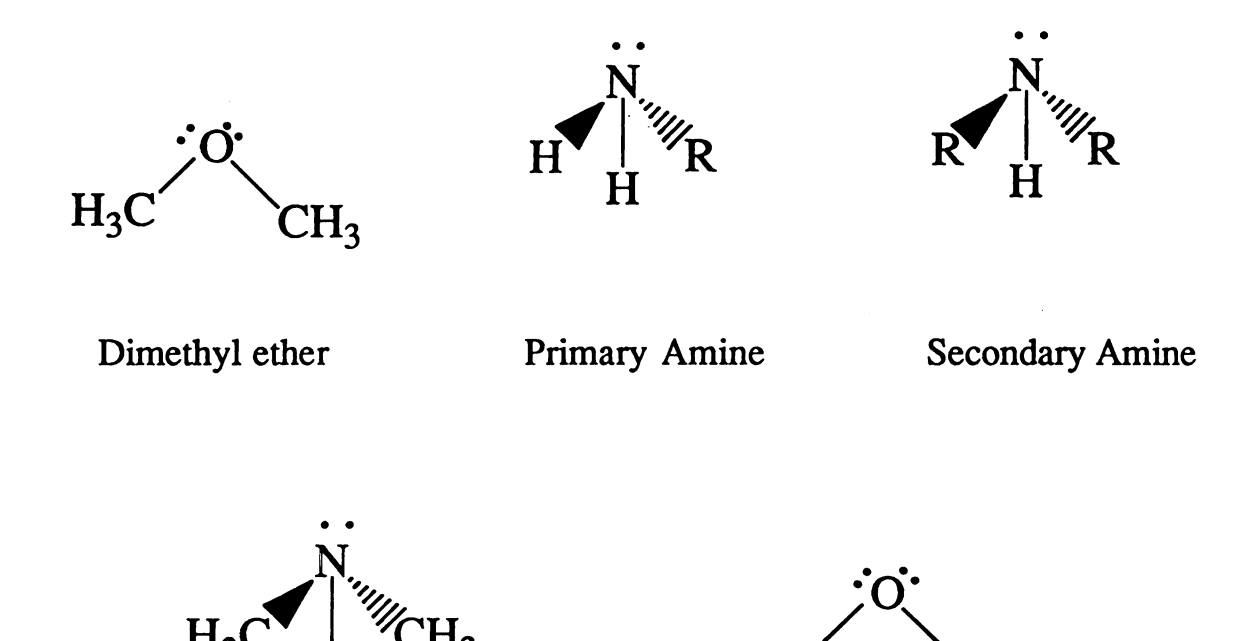


Figure 6: Common organic solvents. The 1° and 2° amines are not as resistive to reduction as the ethers or 3° amine, due to the ionizable protons on the former amines.

Trimethylamine

Diethyl ether

Preparation of Cs+(15C5)(18C6)e-.

The preparation of an electride often requires the use of a K-cell (Figure 7) that is made mostly of quartz (especially when lithium metal is used). This prevents accidental contamination with a sodide when a metal other than Cs is used in the synthesis, due to exchange of the natural Na⁺ in the borosillicate glass of Pyrex with another alkali metal cation in the presence of an electron or M. The synthesis of alkalides does not require a quartz K-cell, except for the case of lithium, because lithium is the most likely alkali metal to exchange with the sodium in glass. Initially, the Kcell was cleaned rigorously to inhibit solution decomposition. The apparatus was partially filled with an aqua regia solution which was composed of three parts HCl and one part HNO3. This was allowed to stand for one day. The following day, the solution was poured out and washed six times with distilled water, followed by six rinses with conductance water. The conductance water was distilled water that had been deionized and redistilled through a high reflux ratio column so that less than 1 ppm of impurity remained. The K-cell was then placed in an oven at around 275°C to completely dry. Sometimes the K-cell apparatus was placed on the vacuum line overnight, with the proper 9 mm Ultra-Torr attachments at points 1 and 2, and evacuated so as to check for any faults in the glass as well as to distill out any water that remained in the Kcell. As is evident from this description, the cleaning process is very important and takes time and patience, so planning an experiment ahead of time is always advantageous.

Once the K-cell had been cleaned and it was determined that it could sustain a vacuum of 10⁻⁵ torr, the K-cell, the appropriate length of a Cs metal ampoule, a spatula and a thistle tube were all placed in the Vacuum

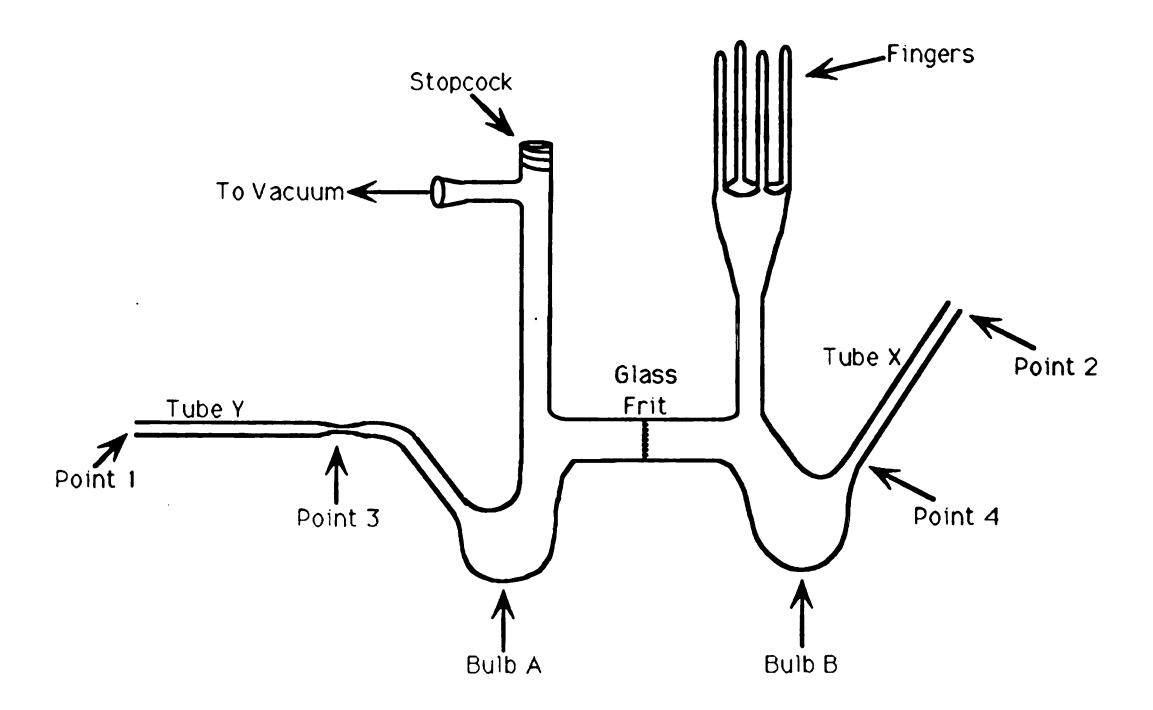


Figure 7: K-cell used in the synthesis of alkalides and electrides.

Atmosphere Company (VAC) Glove Box outer chamber to be evacuated to about 10 mtorr. Once the outer chamber had been evacuated, the equipment could be accessed through the port and brought into the glove box. A metal ampoule of the appropriate length was scored with a knife stored in the glove box and cracked. The portion of the cracked ampoule containing the metal was placed into tube Y so that the sealed part of the ampoule was facing towards the inside of the apparatus (this was done so as to help prevent any bumping of the metal when it was distilled). If the ampoule was cracked in the middle of the Cs metal portion, both parts were placed in the side tube. The Ultra-Torr attachment was then placed securely on the end of the side tube at point 1. Next the complexant was added through point 2 and into bulb B. The thistle tube (15 cm long, 4 mm OD Pyrex tubing with a funnel at the top) was very handy at this point because it helped prevent any of the complexant from adhering to the sides of the tube X. Approximately the same molar amounts of the two complexants were added to the apparatus. When synthesizing an electride, a slight excess of complexant is preferred. The opposite is true in an alkalide synthesis. Once the two complexants had been added to the bulb, the ultra-torr attachment was attached to point 2, and the apparatus was ready to come out of the glove box. It was important to check that the stopcock was closed and that both Ultra-Torr attachments were tightly secured.

Once the apparatus was taken out of the glove box, it was imperative that no oxygen was allowed into the K-cell. At this point, the K-cell apparatus, which contained a He atmosphere, was directly attached to the vacuum line and evacuated. When the pressure had reached 10-5 torr, the apparatus was sealed with a torch at points 1 and 4. Since 15C5 is a

somewhat volatile liquid, a dry ice/isopropanol bath was used to keep the 15C5 cold in order to prevent it from distilling into the cold trap under vacuum. When the two side-arms had been sealed-off, a freshly distilled Cs mirror was deposited into bulb A by using a light flame. A nice gold-colored mirror always formed rather quickly. It was important not to distill the Cs too rapidly or else large balls of metal would form and deposit on the bottom of the bulb. This was not disastrous, but the thinner the film was, the faster the metal could be used in the reaction. It was also important to prevent the metal from depositing too high on the neck of the vessel so as to approach the stopcock. Applying heat near a stopcock is not a good idea anyway, when the importance of a good vacuum is at stake. After the metal had been completely distilled, the stem of the tube was sealed at the narrowed portion of the glass, point 3.

About 10-15 mL. of solvent (Me₂O) was then introduced into bulb B, which contained the two crown ether complexants, through an extended-tee, at about -35°C. In addition to the Me₂O, about 1-2 mL. of methylamine was added to bulb B to aid in dissolving the crown ethers. This process is not customary in general electride synthesis, but was helpful in this particular procedure. It was crucial that the crown ethers were dissolved as completely as possible before allowing the solution to contact the metal mirror. This actually is a rather difficult process because the dimethyl ether has a low boiling point (-24.8°C) so the temperature of the bath cannot be raised too high, but high enough to dissolve the crowns. About -35°C appeared to be a good temperature for this process. Once the complexants had dissolved, the solution was exposed to the mirror (bulb A) and the deep blue color, indicative of solvated electrons was formed immediately. It was important to let the metal react completely with the

complexants so that no metal mirror remained. The amount of Cs that had been added to the reaction vessel was insufficient to react with all of the crown present, in order to prevent the formation of a ceside. A deficient amount of alkali metal was always added during an electride synthesis, so that reaction of all of the alkali metal with complexant was an indication that electride had been formed. This process usually took about a day and a half. Once all of the metal had been dissolved, about 3-5 mL. of TMA was added to bulb A at -78°C. TMA acts as the cosolvent for crystallization of the product. All of the solution was poured through the frit to bulb B and the remaining deep blue mirror was washed very well by using a cotton swab dipped in liquid nitrogen to distill over some clean solvent which was then used to dissolve the mirror. This sometimes took several hours. At this point, the solution was brought to saturation by evaporation of Me₂O. Crystal growth was effected by slow evaporation of the solvents through three additional frits, at -78°C over a period of about a week. It was important to keep the two bulbs and the frit in a dry ice/isopropanol bath throughout the entire procedure since electrides are very sensitive to higher temperatures. Several syntheses yielded only decomposition products because the temperature of the apparatus was not kept extremely cold. During this waiting time, the solution was carefully checked to monitor the progress of crystal formation. When about 5 mL. remained in the bulb and crystals were present, (usually, a polycrystalline material was produced) the remaining solvent was poured through the fritted glass to bulb A and distilled out of the apparatus. The black material that had formed was not necessarily clean material, so it was important to wash it carefully with a cosolvent such as TMA or Et₂O. This entailed adding about 10 mL. of cosolvent to the flask containing the

crystals and decanting through the frit anything that dissolved in the solvent, such as any unused crown. The solvent was then distilled back into bulb B and the procedure was repeated several times until one was confident that the material was free of complexant. Finally, the crystalline material was left to dry on the vacuum line overnight by pumping at about 10^{-6} torr while the K-cell was kept in a dry ice/isopropanol bath.

It is important to note that the cleaning ritual described earlier, was especially important in that it helped eliminate impurities. In addition, by avoiding a fast precipitation of the product, good polycrystalline material is usually produced. By going through this extra trouble, we were allowed to produce crystalline material more consistently.

When the crystals were dry, the entire K-cell was taken off the vacuum line and prepared for flipping of the apparatus so that the crystals would fall nicely into the fingers, which would subsequently be sealed from the apparatus. This preparation entailed placing the K-cell in a large storage container for the dry ice, so that the fingers and bulb B, which contained the electride crystals, were in contact with the cold cubes of dry ice. This was done so that when the crystals came in contact with the fingers, they would not be exposed immediately to a warm surface. Instead, there was no temperature change since both parts of the apparatus were in the same environment. Following this procedure, the fingers were immediately placed in a large dewar containing liquid nitrogen and sealed from the apparatus with a hot flame.

When the time came to transfer the material into an EPR tube, this was performed in a glove bag equipped with a flow of nitrogen gas. A tall dewar containing the samples, a glass cutting knife, the EPR tube (4 mm OD quartz tube attached with a graded seal to a stopcock and vacuum line

joint), a few melting point capillary tubes, and a mortar and pestle, were all placed inside the glove bag through the opening. Typically, about four liters of liquid nitrogen were poured into a large styrofoam dewar in the glove bag to create a large positive pressure of the inert gas in the glove bag which would in turn drive out any air that got in the bag during loading of the appropriate equipment. This process was repeated several times so that all of the air had escaped and the glove bag was then kept cold until the procedure was completed. The mortar was then filled with liquid nitrogen and the sample tube was scored with a glassblower's knife and broken. The contents were poured immediately into the very cold mortar. The crystals were then crushed with the pre-cooled pestle to a very fine powder. A very small amount of the powder was then placed in the capillary tube and the entire capillary tube was then placed into the large EPR tube and kept cold in liquid nitrogen. The reason for using the capillary tubes was that it had been found in previous experiments that when the powder was loaded directly into the EPR tube, a light film would coat the sides of the tube and it was often difficult to collect all of the sample at the bottom of the tube. By using the capillary tubes this problem was eliminated and no further complications were observed. The EPR tube was then placed on the vacuum line, and the quartz tube was immersed in liquid nitrogen and sealed by using a very hot flame, after which it could be used for EPR measurements.

CHAPTER 3 THEORETICAL APPROACH TO ELECTRON PARAMAGNETIC RESONANCE

Electron Paramagnetic Resonance, or EPR, is a sensitive technique for the detection of paramagnetic species 17a,b . The presence of unpaired electrons in atoms or molecules gives rise to a magnetic dipole moment. Classically, the energy of a magnetic dipoles, μ , in a static magnetic field, H, is given by Eq. III-1,

$$E = -\mu \cdot \overline{H}$$

$$\mu = \text{magnetic moment}$$
or
$$H = \text{field strength} \qquad \text{(III-1)}$$

$$E = -\mu \cdot H \cos \theta$$

$$\theta = \text{angle between } \mu \cdot \& H$$

When $\theta = 0^\circ$ and $\mu > 0$, the minimum energy is obtained resulting in a parallel configuration of the dipole for a given value of the magnetic field strength. When $\theta = 180^\circ$, the maximum energy is obtained and an antiparallel configuration of the dipole is obtained with respect to the magnetic field strength.

The static picture presented in Figure 8, is perturbed by the presence of electron spin angular momentum, which causes the moments to precess

about the direction of the applied magnetic field at an angle, θ , determined by the value of the spin angular momentum and in a direction given by: μ x H. Because spin angular momentum is quantized, only certain discrete angles, and therefore, discrete interaction energies for the electron spin with the applied field are allowed. For a system with a single unpaired electron spin, the allowed values for the electron spin angular momentum

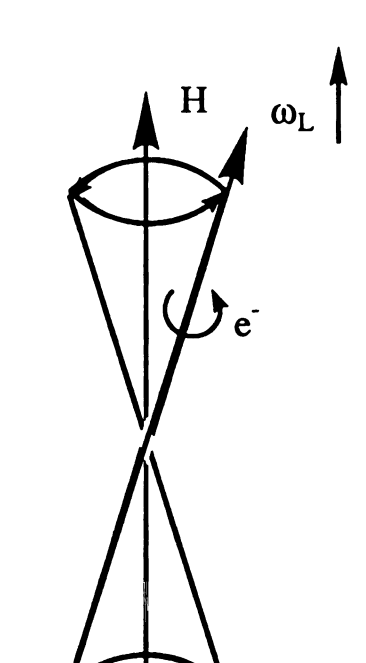


Figure 8: Precession of electronic spin angular momentum and magnetic moment in a magnetic field.

are given by, $M_s \, \hbar$, where M_s is the electron spin quantum number and can take on the values of $\pm 1/2$. The energies of these two states are given by Eq. III-2,

$$E = M_s g \beta H \qquad (III-2)$$

where, g is the Lande' g-factor, β is the Bohr magneton and H is the magnetic field in Gauss. In EPR spectroscopy, the energy difference between these two states (Eq. III-3),

$$\Delta E = g\beta H$$
 (III-3)

is probed, (see Appendix A for a complete derivation). For a typical laboratory magnetic field of 3400 G, ΔE is on the order of 10^{-24} J thus the frequency of the electromagnetic radiation used for this spectroscopy is on the order of 10 GHz, corresponding to the microwave region (Figure 9).

Thus, the interaction of a magnetic dipole with electromagnetic radiation can induce transitions between two Zeeman levels if the photon (hv) equals the separation $g\beta H$.

Since this system has discrete energy levels which are described by well defined quantum numbers, necessarily, an eigenvalue equation can be written. Consider a system where λ_i represents an eigenvalue of a state and ϕ_i represents an eigenfunction or basis set for that eigenvalue. An eigenvalue equation can be written as follows (Eq. III-4)

$$\hat{O}\phi_{i} = \lambda_{i}\phi_{i} \tag{III-4}$$

where $\stackrel{\wedge}{O}$ is the necessary operator for the system. Since EPR deals with spin angular momentum, a spin operator is appropriate here. This spin operator will operate on a function specifically defining a spin state. Consider the system with one unpaired electron, S = 1/2, resulting in two quantum numbers, $M_S = \pm 1/2$. The components $M_S \, \hbar$, of angular momentum along the magnetic field direction are measured by the quantum

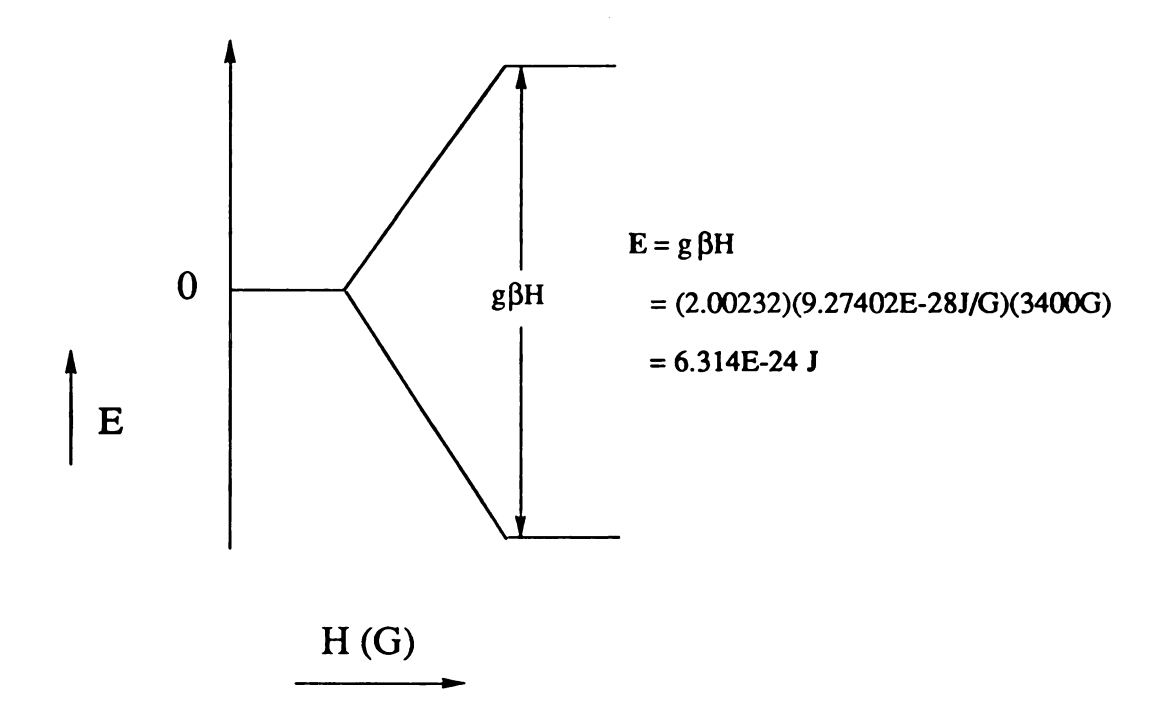


Figure 9: Electron spin levels in a magnetic field.

Resonance is achieved when the frequency of the incident radiation matches the frequency corresponding to the energy level separation.

numbers, M_s . Thus if $\hat{S}h$ is the angular momentum operator, Eqs. III-5, III-6a and III-6b:

$$\hat{S}\phi_{i} = M_{S}\phi_{i} \tag{III-5}$$

or

$$\hat{S}\phi (M_S = 1/2) = 1/2\phi (M_S = 1/2)$$
 (III-6a)

$$\hat{S}_{\phi} (M_S = -1/2) = -1/2 \phi (M_S = -1/2)$$
 (III-6b)

Using the more common notation, Dirac notation and designating the axes of quantization of the angular momentum to be the z-direction, Eqs III-7a and III-7b,

$$\hat{S}_{z} | 1/2 \rangle = 1/2 | 1/2 \rangle \tag{III-7a}$$

If we let α be equivalent to $M_s = 1/2$ and β to $M_s = -1/2$, these expressions can be simplified even more, Eqs. III-8a and III-8b,

$$|1/2\rangle = |\alpha\rangle = \phi_{\alpha} \tag{III-8a}$$

$$|-1/2\rangle = |\beta\rangle = \phi_{\beta}$$
 (III-8b)

M_s is a precise measure of the spin angular momentum components, and the energies associated with such systems are obtained from the Schrödinger equation (Eq. III-9),

$$\mathcal{H}\phi_{i} = E_{i}\phi_{i} \qquad (III-9)$$

where \mathcal{H} is the spin Hamiltonian operator. Eqs III-10a,b then follow,

$$\mathcal{H}|\alpha\rangle = E_{\alpha} |\alpha\rangle \qquad (III-10a)$$

$$\mathcal{H}|\beta\rangle = E_{\beta}|\beta\rangle \qquad (III-10b)$$

It is important to note that operators having the same set of eigenfunctions have a useful property in that they must commute.

It was shown in the Appendix, that $\mu_z = -\gamma M_s \hbar$ thus it may be expected that $\stackrel{\wedge}{\mu_z}$ (the magnetic moment operator) should be proportional to $\stackrel{\wedge}{S_z}$. This results in Eq. III-11,

$$\hat{\mu}_{z} = -\gamma \hat{S}_{z} \hat{\pi} = -g \beta \hat{S}_{z}$$
 (III-11)

Now combine Eqs. III-1 and III-11 resulting in the spin Hamiltonian, Eq. III-12,

$$\mathcal{H} = g\beta H \hat{S}_{z}$$
 (III-12)

An expansion of this can be written as, Eq. III-13a and III-13b,

$$\mathcal{H}|\alpha\rangle = g\beta H \hat{S}_z |\alpha\rangle$$
 (III-13a)
= $1/2g\beta H |\alpha\rangle$

$$\mathcal{H}|\beta\rangle = g\beta H \hat{S}_{z}|\beta\rangle \qquad (III-13b)$$
$$= -1/2g\beta H|\beta\rangle$$

For a transition between α and β , Eq. III-14 expresses the energy difference,

$$\Delta E = E_{\alpha} - E_{\beta} = g\beta H = h\nu. \tag{III-14}$$

thus complying with Figure 9 and the energy level splittings.

The interactions discussed thus far have been between an electron and a magnetic field. If this were the only effect measured by the EPR, all spectra would be relatively indistinguishable as they would only consist of one line. The only useful feature would be the g-value. However, the electron spin magnetic dipole can interact with with nuclei in its vicinity, as some nuclei possess an intrinsic spin angular moment and a magnetic moment associated with it. Magnetic nuclei can produce a local magnetic field, and the interactions between the electron and the magnetic nucleus is the known as the *nuclear hyperfine interaction*. This interaction can be either orientation dependent (anisotropic), or independent of the orientation of the field (isotropic).

Consider a nucleus which has an intrinsic spin, I=1/2. The nuclear hyperfine interaction splits each of the Zeeman levels into two levels (Figure 10). The observed transitions are those obeying the EPR selection rules, $M_S = \pm 1$ and $M_I = 0$.

The Hamiltonian describing the hyperfine interaction follows Eq. III-15.

$$\mathcal{H}_{iso} = hA_o \hat{S}_z \hat{I}_z$$
 (III-15)

where A_0 is the isotropic hyperfine coupling constant, \hat{I}_z is the nuclear spin operator and the measurement of the interaction between an electron and a nucleus is hA_0 . Thus the total Hamiltonian is given by, Eq. III-16.

$$\mathcal{H} = g\beta H \dot{S}_z + h A_0 \dot{S}_z \dot{I}_z \qquad (III-16)$$

Since the energy values of \hat{S}_z are $Ms = \pm 1/2$ and for \hat{I}_z , $M_I = \pm 1/2$, four possible spin states are obtained (Eq. III-17),

$$\begin{split} & |\alpha_e,\,\alpha_n\rangle & |\beta_e,\,\alpha_n\rangle \\ & |\alpha_e,\,\beta_n\rangle & |\beta_e,\,\beta_n\rangle & (\text{III-17}) \end{split}$$

and can be further related (Eqs. III-18a, III-18b),

$$\hat{S}_z | \alpha_e, \beta_n \rangle = 1/2 | \alpha_e, \beta_n \rangle$$
 (III-18a)

$$\hat{I}_{z}|\alpha_{e},\beta_{n}\rangle = -1/2|\alpha_{e},\beta_{n}\rangle \qquad (III-18b)$$

Thus the energies for these states can be obtained, Eq. III-19

$$E_{\alpha_{e}\beta_{n}} = \langle \alpha_{e}, \beta_{n} | \mathcal{H} | \alpha_{e}, \beta_{n} \rangle$$

$$= \langle \alpha_{e}, \beta_{n} | g \beta H S_{z} + h A_{o} S_{z} I_{z} | \alpha_{e}, \beta_{n} \rangle$$
(III-19)

$$= 1/2g\beta H - 1/4hA_0$$

and the energies for the other states are obtained similarly (Eq. III-20),

$$\begin{split} E_{\alpha_e\alpha_n} &= 1/2g\beta H + 1/4hA_o \\ E_{\beta_e\alpha_n} &= -1/2g\beta H - 1/4hA_o \\ E_{\beta_e\beta_n} &= -1/2g\beta H + 1/4hA_o \end{split} \tag{III-20}$$

This same procedure is followed for a system where I = 1. In this case, there are six spin states (Eq. III-21),

$$|1/2, 1\rangle$$
 $|-1/2, 1\rangle$
 $|1/2, 0\rangle$ $|-1/2, 0\rangle$ (III-21)
 $|1/2, -1\rangle$ $|-1/2, -1\rangle$

Similarly to Eq. III-19, the energies can be obtained. The interactions between an electron and a nucleus (I = 1/2), are easiest viewed in an energy level diagram (Figure 10).

Now that a general background of EPR theory has been discussed, it is worthwhile to mention the instrumentation. A typical EPR spectrometer (Figure 11) consists of the following components: a magnet, a cavity (which contains a set of Helmholtz coils) to contain the sample, a source of microwave radiation, a detection system, and signal processing and signal enhancement electronics. When the resonance condition is satisfied, microwave power is absorbed by the sample. Because the experiment is carried out with a fixed source frequency, the spectrum is generated by measuring the microwave power absorbed by the sample as a function of

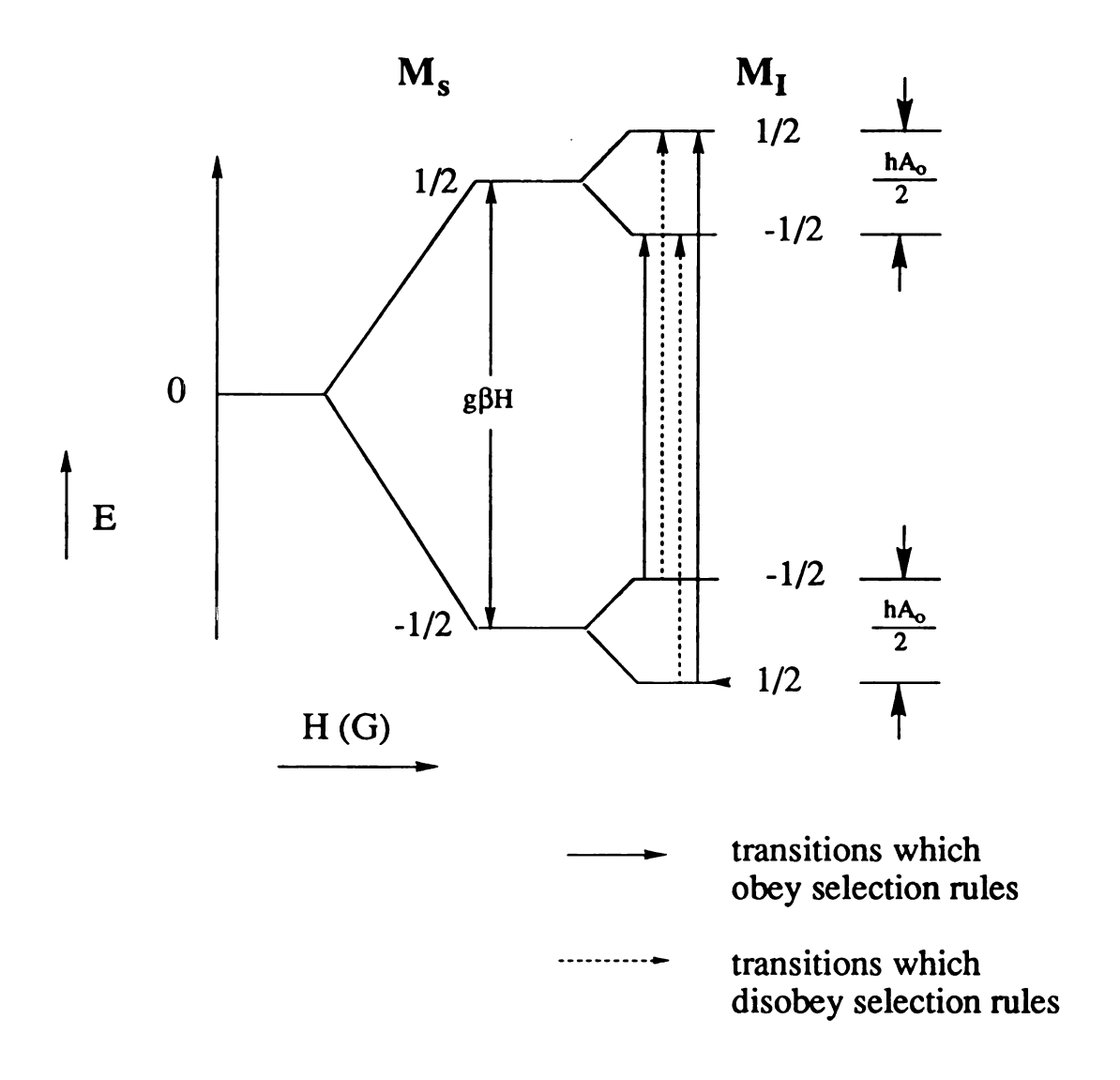


Figure 10: Energy level diagram describing the effect of nuclear hyperfine interactions.

the the magnetic field strength. Monochromatic radiation is derived from a klystron. The frequency of this radiation is adjusted so that standing waves are set up in the sample cavity. The sample is placed into a region of the cavity where the microwave magnetic field is at a maximum. The sensitivity of the experiment is determined, in part, by the quality factor, or Q, of the cavity. An expression for Q is given in Eq. III-22.

$$Q = 2\pi (E_{\text{stored}}/E_{\text{dissipated/cycle}})$$
 (III-22)

Essentially, microwave radiation in the cavity makes "Q" passes through the sample before it exits to the detector. Microwave energy is physically coupled into and out of the sample cavity by a small hole called the *iris*. The signal is then deflected to the crystal detector and eventually, the signal can be viewed on the oscilloscope or recorded. The phase sensitive detection technique utilizes small amplitude magnetic field modulation to "package" the EPR signals with a specific carrier frequency and then amplifies and detects only signals occurring at that frequency. Because noise occurs at random frequencies, this procedure enhances the signal-to-noise ratio of the measurements by eliminating much of the noise. The advantage of phase sensitive detection is the increase in sensitivity, but as a result, the signal will appear as a first derivative.

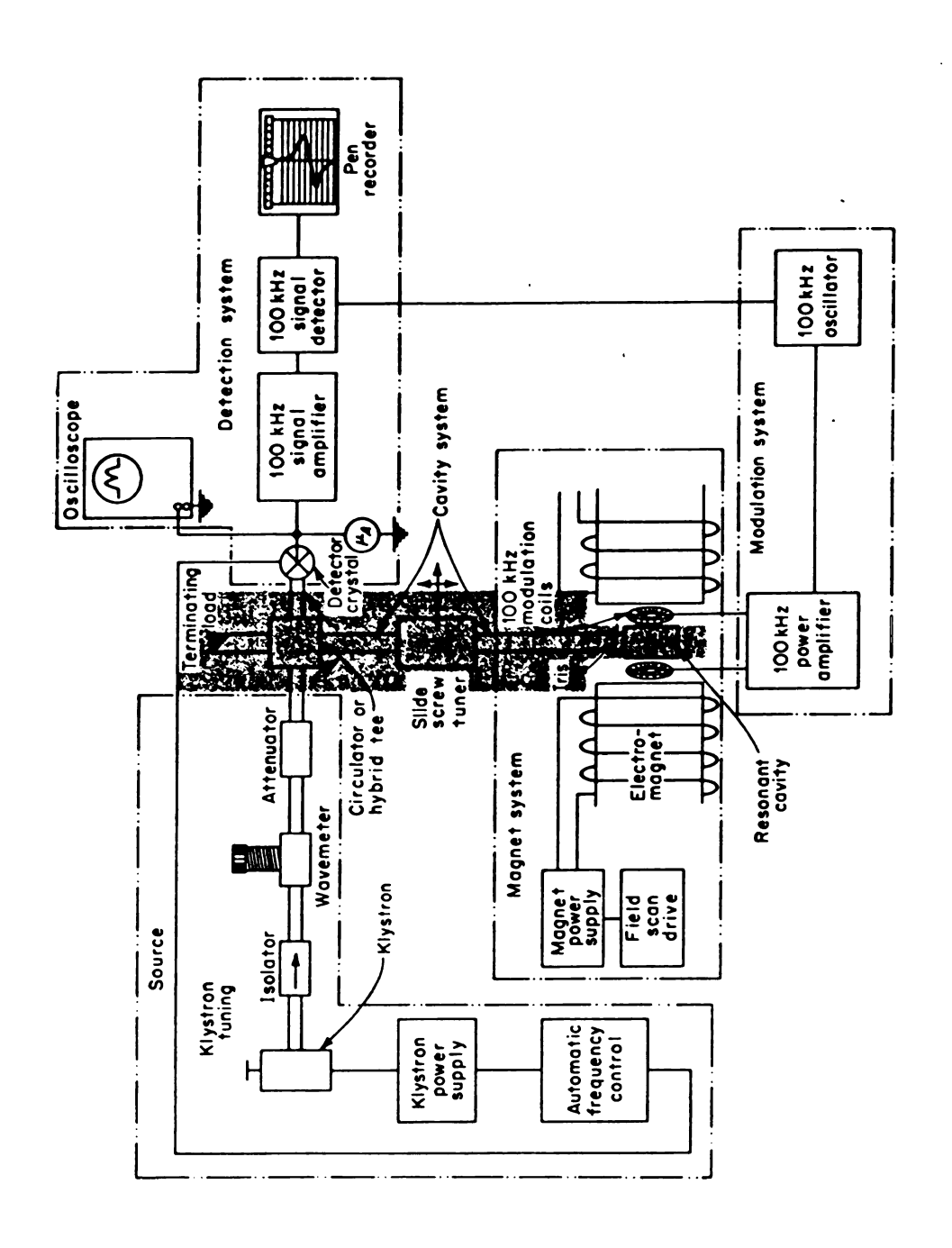


Figure 11: Schematic Drawing of a CW-EPR Spectrometer.

CHAPTER 4

EPR Results and Discussion of Cs+(18C6)(15C5)e- and Li+(C211)e-

$Cs+(15C5)(18C6)e^{-}$

EPR studies were performed on Cs+(18C6)(15C5)e- to obtain additional information regarding the electronic interactions of this system. A Bruker ER-200D spectrometer operating at X-band was used for these experiments. The temperature was controlled by using a cold stream of nitrogen gas through a transfer line connected indirectly to the TE₁₀₂ rectangular cavity, and the temperature was calibrated with a copperconstantan thermocouple with an Omega model 199 digital readout system. An ER350 NMR gaussmeter was used to measure the magnetic field with 1 mG resolution. The g-value was measured directly from magnetic field and frequency measurements. The data were collected with an IBM-AT computer.

The Cs+(18C6)(15C5)e-sample was transferred into an EPR tube as previously described. The temperature in the EPR cavity, was changed about every 8 degrees from roughly 90K to 200K, depending on the particular experiment. The sample was never moved once inside of the cavity, so as to prevent any inconsistencies in the positioning of the tube with respect to the microwave radiation. The resulting spectrum (Figure 12), was a narrow line with a g-value of 2.0019. No resolved hyperfine splitting was observed and the peak to peak linewidths varied from 1.34 G

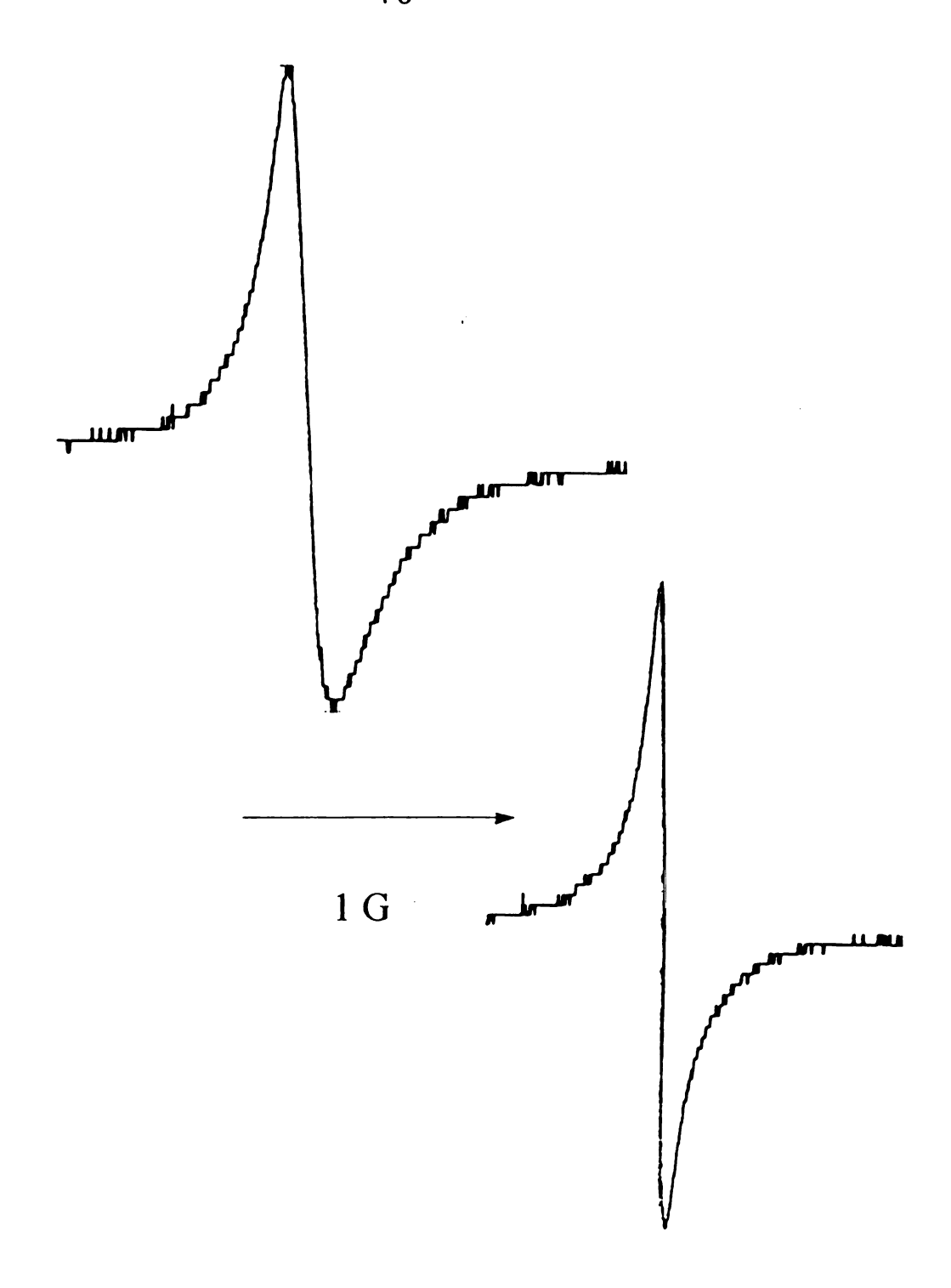


Figure 12: CW-EPR spectra of Cs+(18C6)(15C5)e⁻ at temperatures of 91K (top spectrum) and 221K (bottom spectrum).

at 91 K to 0.965 G at 221 K.

The instrumental settings were kept constant throughout the temperature changes, except for the gain because the intensity of the line became weaker as temperature was increased. Relative intensities were obtained to account for the differences in this factor. Table 2 shows the parameters obtained from the EPR data.

The most accurate way to determine the intensity of an EPR line is to integrate the first derivative spectrum twice. This can be a very tedious procedure however, without the proper computer software. If the linewidths of two components are equal, then peak-to-peak amplitudes of the derivative lines will be proportional to their intensities. However, if the linewidths are different, a modification is needed to obtain the approximate relative intensities from this expression ^{17a} (Eq. IV-1)

$$I \propto Y_{\text{max}} (\Delta H_{\text{pp}})^2$$
 (IV-1)

I represents the intensity of the line, $2Y_{max}$ is the peak to peak derivative amplitude and ΔH_{pp} is the peak to peak width, thus the peak to peak derivative amplitude is inversely proportional to the linewidth squared for a given intensity. For more precise determinations of the EPR line intensities, a double integration of the first derivative EPR signal was performed using the program Spectra Calc. A plot of Intensity vs. 1/T revealed a nearly straight line but the intercept at $1/T = \infty$, is negative. Thus the compound has behavior similar to the Curie Law (Figure 13) in the temperature range of 91K - 221K but not the expected intercept. If the Curie Law were exactly followed, the concentration of unpaired spins would be constant within this temperature range. The EPR results suggest

TABLE 2
EPR Results for One of Three Samples of
Cs+(18C6)(15C5)e-

Rel Intensity	T(K)	1/T(K)	A/B
185428	91	1.10E-02	1.51
140624	101	9.90E-03	1.49
118461	121	8.26E-03	1.57
100755	131	7.63E-03	1.69
83656	141	7.09E-03	1.75
68019	151	6.62E-03	1.82
51834	161	6.21E-03	1.74
38441	171	5.85E-03	1.50
25793	181	5.52E-03	1.32
23432	191	5.24E-03	1.12
17634	201	4.98E-03	1.01
15105	211	4.74E-03	1.09
10002	221	4.52E-03	1.15
10244	231	4.33E-03	1.01
16197	241	4.15E-03	0.90
18026	222	4.50E-03	1.08

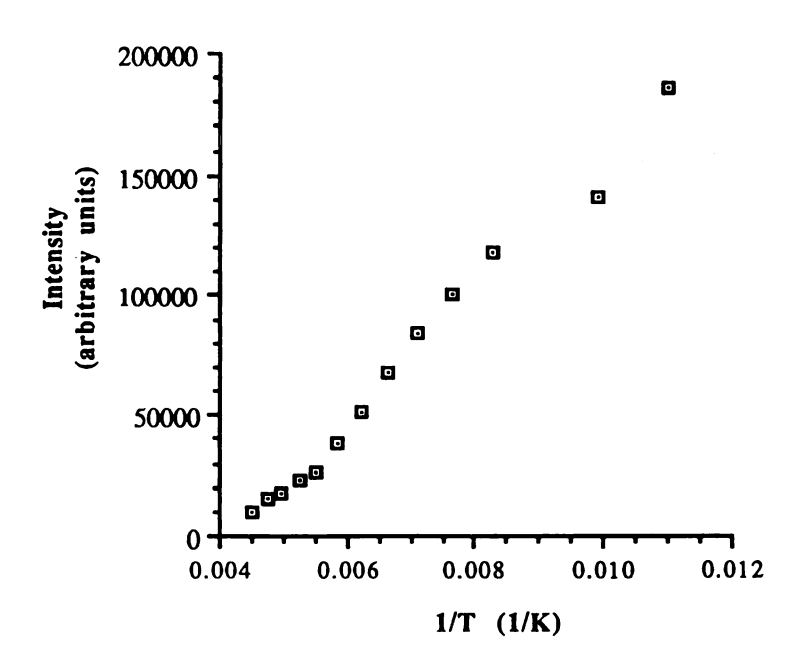


Figure 13: Relative Intensity vs. Reciprocal
Temperature (1/K) for
Cs+(18C6)(15C5)e-

a decrease in the number of spins as the temperature is increased. Interestingly, however, when the temperature was raised to 241 K, the relative intensity increased, in contrast to the previous recordings. In addition, when the temperature was lowered back to 221 K, the relative intensity of the EPR line had *greatly increased* relative to the intensity of the line recorded at the same temperature, only moments before (refer to Table 2). This observation was noted with two of the three samples, (it was not attempted with the third). This effect could be due to thermally induced electron-pair dissociation above 221K, with slow recombination. It could also result from thermally induced decomposition. It should be noted that similar strange time effects were seen in the susceptibility studies.

The magnetic susceptibility results show that this compound has a very small fraction of unpaired spins. When $1/\chi$ vs. T (K) is plotted, the results do not exhibit a straight line over the same temperature range that the EPR results were obtained. Thus these results do not obey the Curie Law. However, at very low temperatures, magnetic susceptibility obeys the Curie Law. The susceptibility also depended on sample preparation but the results in any case did not point towards the Curie Law in the higher temperature range. Thus both susceptibility and EPR indicate deviation from a constant number of spins. It should be noted that *spin* susceptibility is measured in EPR whereas *bulk* susceptibility is measured in magnetic susceptibility experiments, so it is possible that the EPR results do not convey the major contributions to the susceptibility. These other contributions could have been broadened out, or perhaps they arise from a triplet state which was not observed in the EPR spectrum.

The analysis of the NMR results did not follow Curie's Law either. A plot of the chemical shift versus T, over the temperature range comparable to that of the EPR measurements, yielded a relatively straight line with a positive slope. This indicated that as the temperature is raised, the number of spins increases, which once again does not agree with the EPR results, except those at the highest temperature.

The A/B ratios (Table 2) from the EPR spectra were measured for these electrides and the results are plotted vs. inverse temperature (Figure 14). This plot did not show a monotonic pattern in the A/B ratios with respect to the temperature. The increase in this ratio with increase in temperature could be due to an increase in the microwave conductivity. The abrupt decrease at 160K - 190K could be indicative of a phase transition or "softening" mode that also affects the spin susceptibility. The lineshapes that were observed in these spectra, were not purely Gaussian or purely Lorentzian, or even a combination of the two lineshapes. It appears that the lineshapes have some Dysonian character. The Dysonian lineshape 18, which is a characteristic EPR lineshape in metals, depends on several parameters. These parameters are: T_D, the time it takes for an electron to diffuse through the skin depth (δ) , T_T , the time it takes for an electron to traverse the sample, T_1 , the electron spin lattice relaxation time, and T2, the electron spin-spin relaxation time. The Dysonian line has a characteristic about it in that the lower portion of the line and the upper portion of the line are not symmetric, in fact, the upper portion amplitude (low field) is at least 2.6 times that of the lower portion for a metallic sheet. This is referred to as the A/B ratio. However, Webb extended this theory for use with spherical particles in the region of the normal skin effect¹⁹. Webb concluded that metallic particles whose radii, r, are large

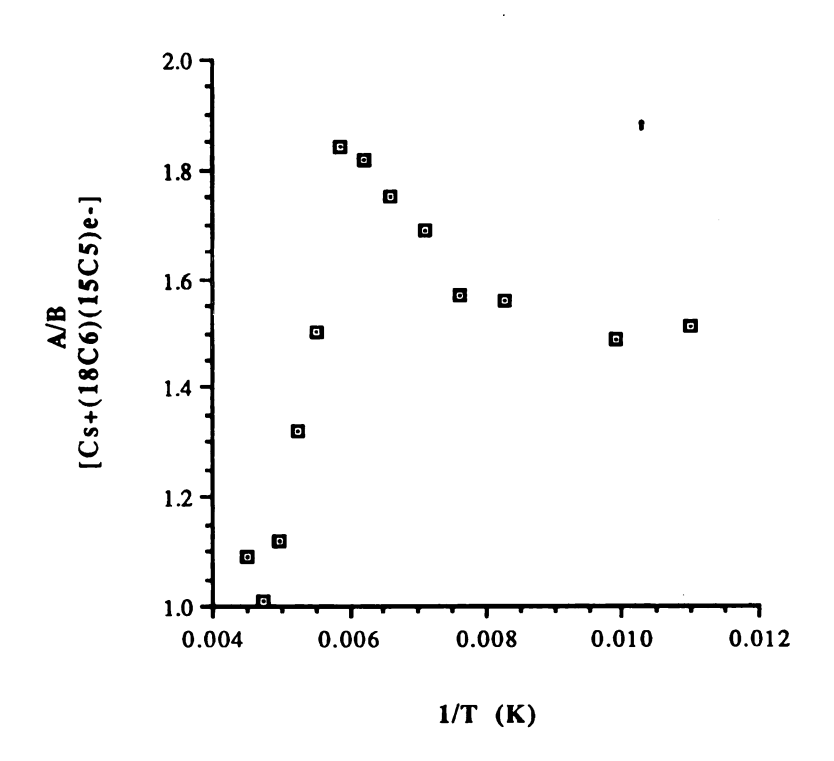


Figure 14: Asymmetry of Lineshape with

Respect to Inverse Temperature (1/K)

compared to δ , will still have a nearly symmetric EPR signal where A/B \approx 1, if $T_D >> T_1$. Therefore, even though the sample may be metallic, if the sample particle size is small compared to the skin depth, or the relaxation time is very short, the EPR signal will be nearly symmetric.

The fact that this electride was found to have a conductivity band gap of only 0.06 eV, suggests that it is possibly a low band gap semi-conductor, or a metal. Due to the small band gap, there may be an accessible triplet state; however there is no direct evidence for this.

The mixed sandwich electride has now been characterized by a variety of methods and a summary and comparison can now be made to two other similar electrides, namely, Cs+(18C6)₂e⁻, and Cs+(15C5)₂e⁻. This is most easily understood by means of a summary table (Table 3).

In addition, both the Cs+(18C6)₂e- and the Cs+(15C5)₂e-, were found to be the first cases of ionic conductors, rather than electronic conductors, whereas the band gap of the mixed sandwich, Cs+(18C6)(15C5)e-, was very small, indicative of a small-gap semi-conductor, or possibly even a metal with grain boundary resistance. The NMR chemical shift of the mixed sandwich was intermediate between the two other sandwich compounds discussed here. Magnetic susceptibility results at low temperatures (below 60K) showed Curie Law behavior for earlier samples of Cs+(18C6)₂e- and for quenched samples of Cs+(18C6)(15C5)e-, but the results for Cs+(15C5)₂e- were dependent on whether or not the system was quenched or annealed. Recently, the earlier results on Cs+(18C6)₂e- have been called into question and appear to have resulted from the inclusion of small amounts of Cs- or solvent. This phenomenon is still under study. The results from the EPR measurements showed that the two "parent" compounds followed Curie's Law. In other words, there was no change in

TABLE 3
COMPARISONS OF Cs+(18C6)₂e-, Cs+(15C5)₂e-, and
Cs+(18C6)(15C5)e-

Sample	Magnetic Susceptibility	EPR	NMR	Apparent band gap conductivity	Crystal Symmetry
Cs+(18C6) ₂ e-	C-W paramagnet with no spin pairing*	Follows Curie's Law	Below 250K, δ is linear with 1/T	>1.0 eV	monoclinic
Cs ⁺ (15C5) ₂ e ⁻	C-W down to 2K after quenching. After anneal, antiferromag behavior	C-W paramagnet	Below 240K, δ is linear with 1/Γ	at least 1.0 eV	triclinic
Cs+(18C6)(15 C5)e-	Follows Curie's Law below 60K. Above 60K, the susceptibility increases.	Follows Curie's Law except at higher temperatures	Susceptibility increases with increasing T.	0.06 eV	monoclinic

^{*}Recently, M. Wagner has shown that an antiferromagnetic transition occurs at ≈ 50K for carefully crystallized samples.

the number of active paramagnetic centers within the temperature range studied. These results correspond well with the susceptibility studies of Cs+(18C6)₂e- and Cs+(15C5)₂e- (if the sample was quenched), however, the results are not so clear-cut with the mixed sandwich. This has already been attributed to the fact that some of the contributions to the susceptibility may be EPR silent. This is apparently not the case with the other electrides in this study.

Finally, the biggest difference among these three compounds is the powder conductivity results. The apparent band gaps of Cs+(15C5)₂e- and Cs+(18C6)₂e- are at least 1.0 eV, which is drastically different from that of Cs+(18C6)(15C5)e- which has a very small band gap of 0.06 eV. Overall, this mixed sandwich electride is primarily spin-paired and the defect electrons may obey the Curie Law at low temperatures, but with deviations markedly at higher temperatures.

Li+(C211)e-

The EPR measurement methods were the same as described above. Previous studies have indicated that below 200K, spin pairing occurred and above this temperature, Curie-Weiss behavior was obeyed. The EPR spectrum obtained in this study, was a narrow line with a linewidth of 0.48 G at 91K and 0.35 G at 219K (Figure 15). The intensities of the spectra were found to very scattered over the temperature range from 91K to 219K as shown in Figure 16. At 219K, the EPR spectrum was recorded twice and yielded different results. The first spectrum was measured as a continuation of the previously increasing set of temperatures, where the temperature initially was brought down to 91K quickly. After the measurement at 219K, the temperature was increased again up to 239K

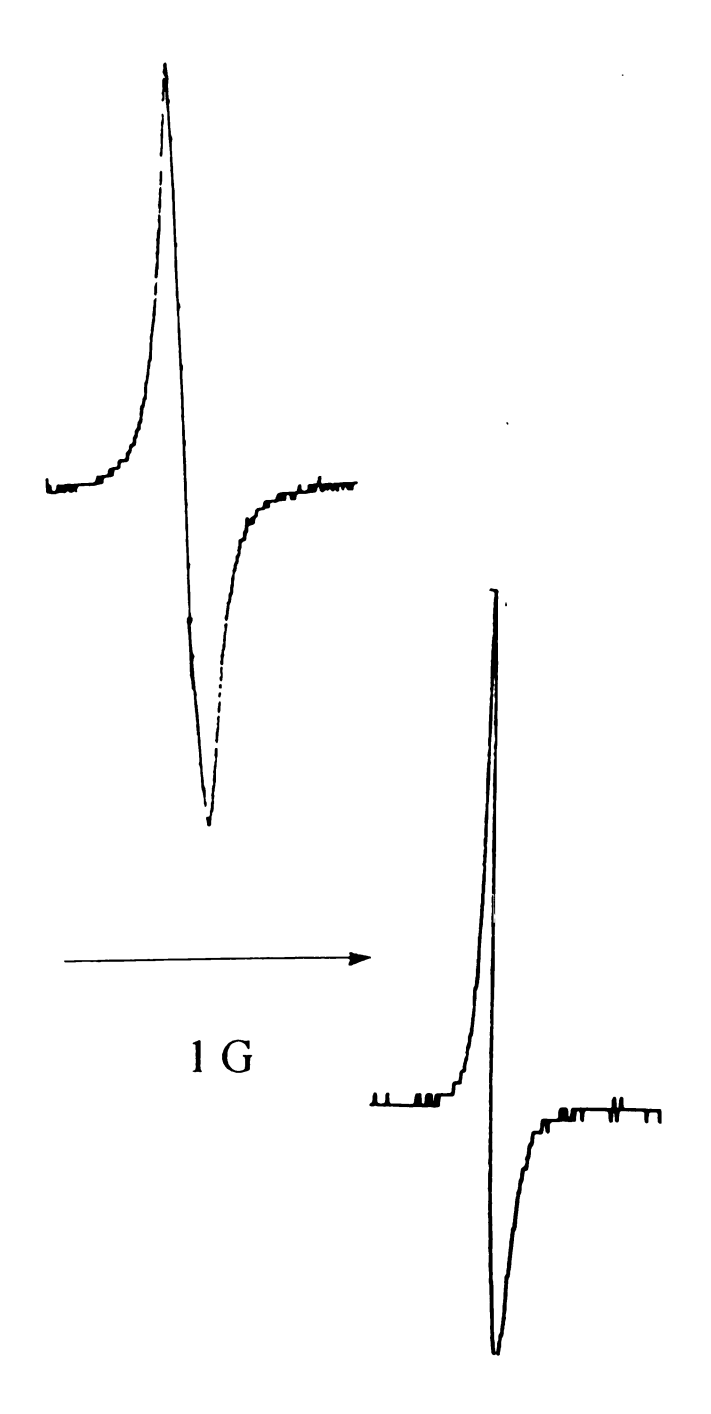


Figure 15: CW-EPR spectra of Li⁺(C211)e⁻ at temperatures of 90K (top spectrum) and 220K (bottom spectrum).

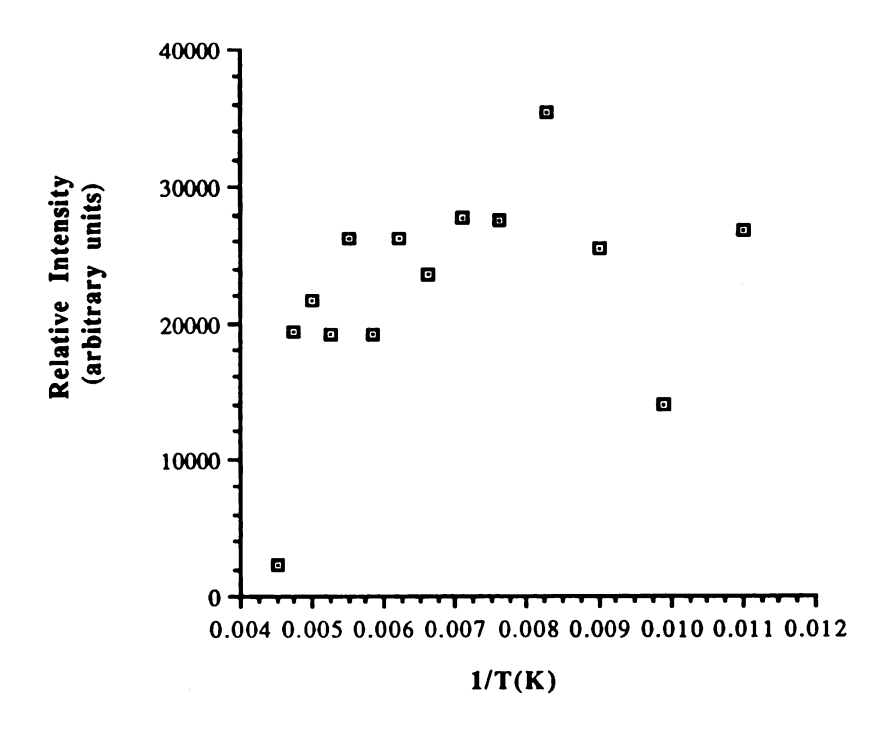


Figure 16: Intensity vs. 1/T (1/K) from EPR
Results of Li⁺(C211)e⁻

(this high of a temperature often results in decomposition of electrides). The intensity increased at this temperature and as the temperature was lowered back down to 219K, the intensity was not the same as previously recorded. Once again, (this same effect was observed in the Cs+(18C6)(15C5)e⁻ sample) the intensity was larger, so perhaps partial decomposition had occurred at around this temperature.

The crystal structure data revealed a large cavity with an estimated diameter of 4.3Å^{15b}. These cavities form open channels along the y-axis of the crystal with a distance between cavities of about 8Å. Smaller channels are exhibited along the z-axis. It is possible that these electrons are more strongly coupled than those in Cs+(15C5)₂e-, which shows electron localization and Curie-Weiss behavior above 4.5K, but weaker than those in K+(C222)e- which shows complete electron pairing. The optical absorption spectra and magnetic susceptibility data, are in agreement with this proposed behavior. The EPR results described here indicate the serious problems with stability and will have to be repeated. Experience has shown that Li+(C211)e- is the most thermally unstable compound we have ever handled. It appears that another sample-loading technique will be required to avoid decomposition.

CHAPTER 5

IN THE FUTURE...

I. Advanced EPR studies of some HMHCY sodides.

Although electron trapping at anionic sites is assumed in alkalides and electrides, the only direct experimental evidence supporting this assertion for electrons trapped in alkalides has come from the cw-EPR and ENDOR experiments, mentioned in Chapter One, for the alkalide series: Cs+(HMHCY)Na-, Rb+(HMHCY)Na-, and K+(HMHCY)Na-. Further characterization of the electron-trapping sites of these three alkalides is proposed. The specific aims of this research are to better define the site at which electrons are trapped in these materials, to gain a detailed understanding of how the unpaired electron spin density is delocalized over their molecular framework and how this delocalization depends on alkalide structure. These studies will be addressed by using the ESEEM technique^{20a,b} to measure weak, superhyperfine couplings between the paramagnetic center and nearby magnetically-coupled nuclei that are unresolved in the cw-EPR experiment due to inhomogeneous broadening of the resonance lineshape. This research will focus on the complete characterization of the magnetic couplings between the various group 1A metals and magnetic nuclei in the complexant molecules that are coupled to trapped electrons in these materials. The HMHCY sodides have been chosen for this study because of their enhanced thermal stability as

compared to that of other alkalides and electrides and because of their extensive characterization by x-ray crystallography, cw-EPR⁶ and ENDOR techniques^{21a,b}. Furthermore, cw-EPR studies done on the series, Cs+(HMHCY)Na-, Rb+(HMHCY)Na-, K+(HMHCY)Na-, show that the couplings between the paramagnetic center and the closest alkali metal cation in these materials is dependent on the alkalide structure.

ESEEM studies will be performed at different microwave frequencies from 6-18 GHz. The superhyperfine interactions will also be measured, between the trapped electrons and the magnetic nuclei of the surrounding complexant molecules focusing initially on the ¹⁴N couplings. These initial studies will be followed by experiments on HMHCY sodides where the complexant is labeled with ¹³C and /or ²H. Together, the results of these experiments should provide the most accurate information regarding the "structure" of the electron trapping site obtained to date.

ESEEM

Different local fields surrounded by unpaired electrons in a sample give rise to inhomogeneous broadening. A cause of this type of broadening is from dipolar interactions between spins with different Larmor frequencies, or from magnetic anisotropy. A spin packet is a group of spins that see the same local field in the sample and can be visualized in Figure 17.

Each spin packet has a Lorentzian lineshape but the overall envelope has a gaussian lineshape. Figure 17 represents the inhomogeneously broadened line. A homogeneous system would consist of only one spin packet of Lorentzian lineshape and this type of broadening can be caused from spin lattice relaxation, dipole-dipole interactions between like spins,

and spin interactions with the microwave field. Inhomogeneously broadened lines can mask the hyperfine structure in an EPR spectrum, so this type of broadening often results in a loss of resolution in the spectrum, and to unresolved hyperfine structure.

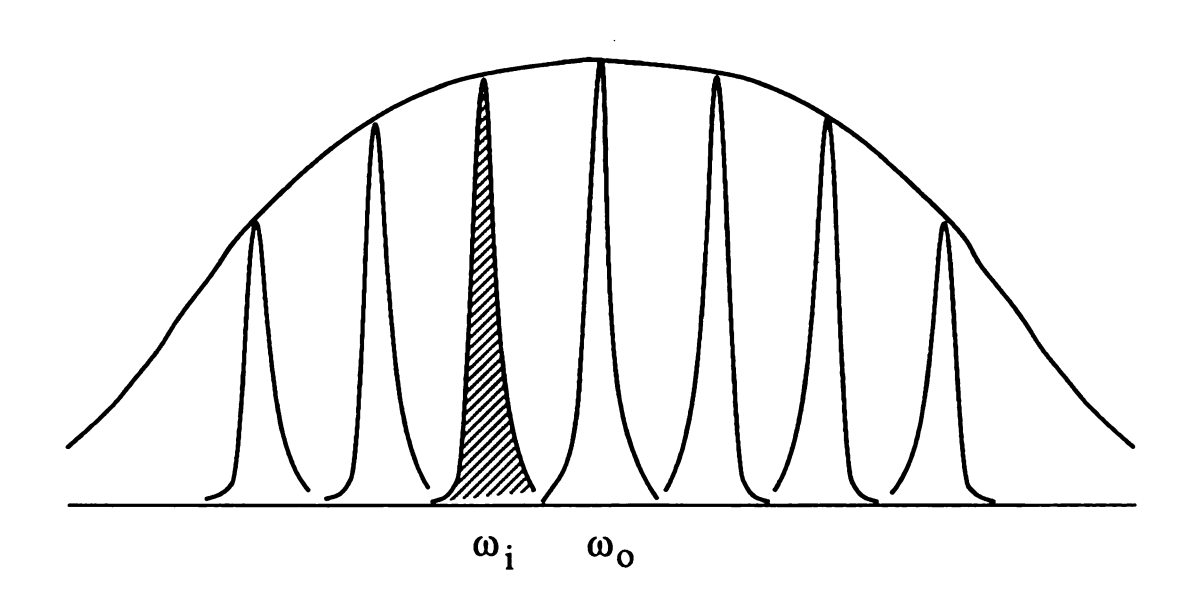


Figure 17: Individual spin packets which are homogeneously broadened, enveloped by an inhomogeneously broadened line.

Inhomogeneous broadening can be reversed by performing a spinecho experiment. As was noted in the discussion on cw-EPR, electrons can assume either a parallel or anti-parallel configuration when in an external magnetic field. A Boltzmann distribution describes the populations of the β state (lower in energy) and the α state. The resulting magnetization, M_z , is established in the direction parallel to the magnetic field, H_o . The magnetization changes upon application of a pulse, and this is best described by a vector diagram, using a coordinate system which rotates with a frequency ω_{mw} (Figure 18).

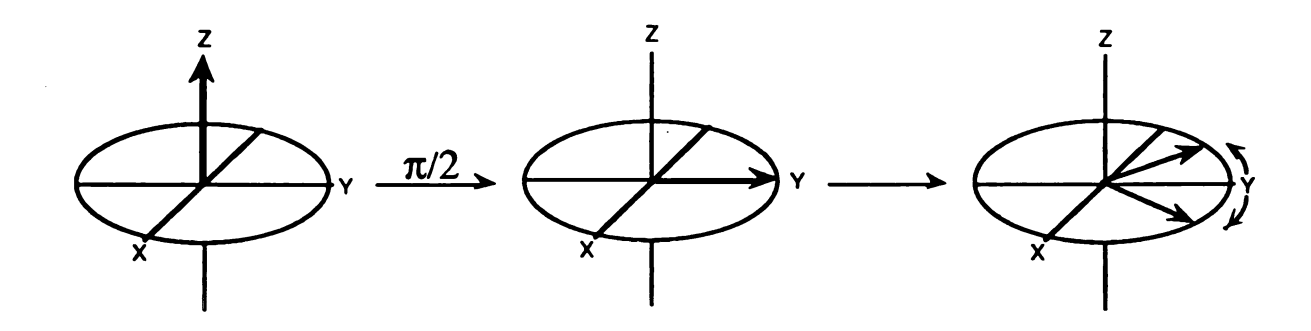


Figure 18: Evolution of the magnetization during a single $\pi/2$ pulse

The result of applying a $\pi/2$ pulse, the duration of which is dependent on the strength of the microwave magnetic field, is a rotation of the magnetization through a flip angle, β , in the plane perpendicular to the x-axis, where $\beta = \gamma_e H_1 t_p$ where γ_e is the gyromagnetic ratio (or magnetogyric ratio), H_1 is the field intensity of the microwave pulse and t_p is the duration time of the pulse. In this case, the flip angle, β , is $\pi/2$, but this is only the simplest case. Virtually any sequence can be used. The single $\pi/2$ pulse transforms the original longitudinal magnetization, M_z , into a transverse y-magnetization. It is worth noting that the flip angle is most commonly specified with respect to the on-resonance magnetization. This means that the $\pi/2$ pulse turns M_z into the y-direction exactly 90°. If there were off-resonance components as well, there would be x-components and z-components following the $\pi/2$ pulse. These components

are said to be unimportant for basic pulsed EPR spectroscopy. Therefore, if we assume that the resonance condition, $\omega_{mw} = \gamma_e H_0$, is true, after the $\pi/2$ pulse, all of the magnetization remains in the y-direction. A precession will occur about the z-axis if the Larmor frequency ($\gamma_e H_0$) does not equal the microwave frequency. The precessional frequency, Ω , will be equal to $\omega-\omega_{mw}$. Since the detector is aligned in the direction of the y-axis, the difference frequency is directly measured.

In an ESEEM experiment, a $\pi/2$ pulse yields a magnetization in the y-direction. Immediately after this pulse, the transverse magnetization vectors, or spin packets, begin to precess with their frequencies Ω_i The signal that is observed in the time domain, is a sinusoidal oscillating signal known as a free induction decay, or simply an FID, so the precession results in an FID which decays rapidly. After a certain amount of time, the FID will disappear completely and there is no detectable signal. A time τ , is taken before the second microwave pulse turns the spin packets 180° about the x-axis. At this point, the directions of precession of the individual spin packets will remain the same, so at an additional time τ , the spin packets refocus in the -y direction. The resulting -y magnetization will build up and decay again within a short time and is referred to as the spin echo. This is also called the backfolded FID (Figure 19). This twopulse scheme has an echo amplitude associated with it which is a function of the pulse interval, τ . The decay of the spin echo amplitude is modulated by anisotropy in the hyperfine coupling and is characterized by T_M, the phase memory time or the time it takes for the echo amplitude to decay to 1/e of its initial value.

EPR spectra are often poorly resolved. Consequently, the spin echo shows little structure. As a result, the echo amplitude is used as the main

source of information in ESEEM experiments. The static field strength, H_o, and the time interval between each microwave pulse are variables upon which the amplitude depends. Modulation effects on the amplitudes of the echoes will now be treated.

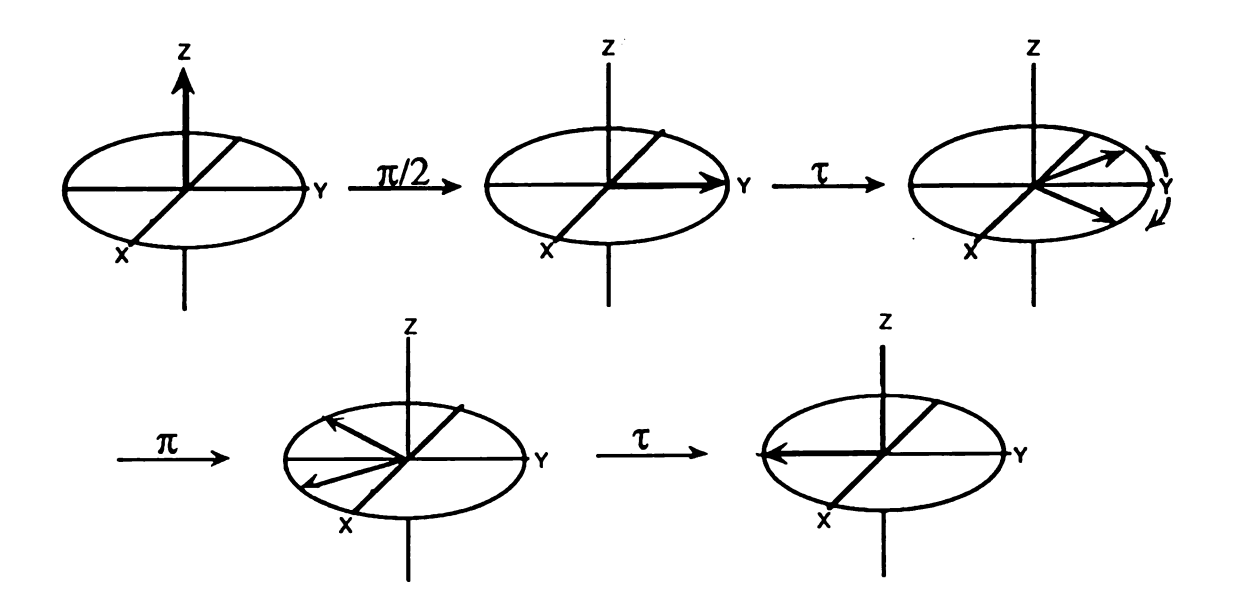
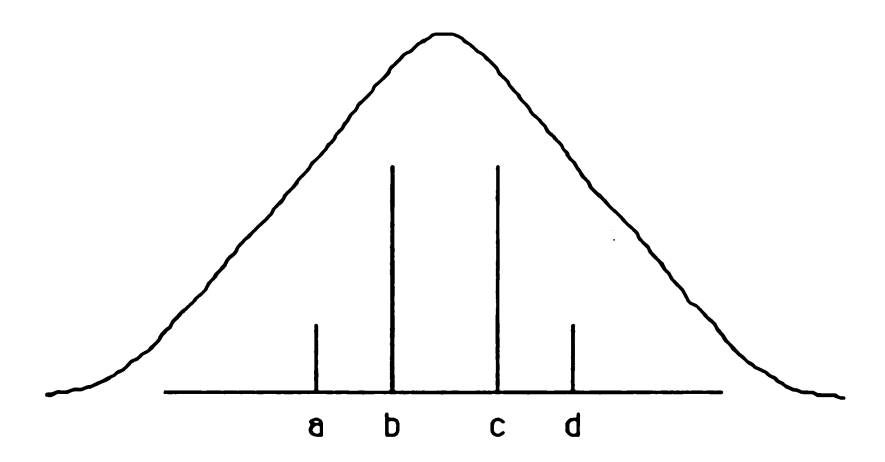


Figure 19: 2-pulse echo sequence and evolution of the magnetization.

Nuclear Modulation Effect

As just described, the couplings between the nuclear spin and the electron spin can cause a modulation of the echo intensity. It is useful to revert back to a cw-EPR experiment with I = 1/2 and S = 1/2, via anisotropic hyperfine interactions. If the hyperfine interactions were only isotropic, only the usual EPR transitions would be allowed (Figure 20). The nature of the anisotropic interactions of the nuclear spin states are



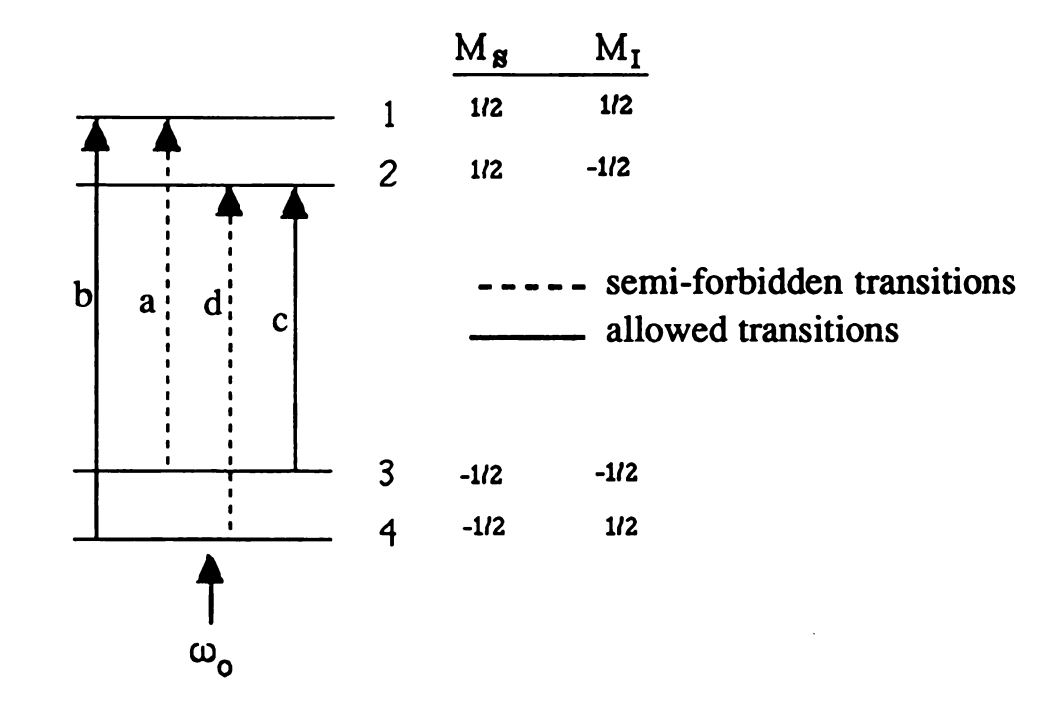


Figure 20: Allowed and semi-forbidden transitions in EPR spectrum.

mixed, and therefore the transitions 1,3 and 2,4 are only "semi-forbidden". Echo modulation is best understood by using a vector diagram (Figure 21). Pay close attention to the pairs of transitions that originate from the same energy level (e.g. $\omega_{1,3}$ and $\omega_{1,4}$). Assume that the resonant frequency of the allowed transition, $\omega_{1,4}$ is equivalent to that of the microwave frequency (i.e. $\omega_{1,4} = \omega_{mw}$). Upon application of short microwave pulses (a large frequency spread), all transitions are excited simultaneously. The microwaves can induce transitions at one level but end at a different level. This is called branching of transitions, and is essential for the nuclear modulation effect.

During the first evolution period following the $\pi/2$ pulse, the orientation of vector 1 remains unaffected, (Figure 21a) whereas vector 2 precesses with a frequency $\omega_2 = \omega_{1,4} - \omega_{1,3}$. After the time interval, τ , the π pulse turns vector 1 into the -y direction as well as giving rise to a new component 2' due to nuclear state mixing and branching of the transitions, (Figure 21b). The same behavior is observed for vector 2, resulting in a new vector 1'. During the second evolution period, vectors 1 and 1' remain unaltered, while vectors 2 and 2' precess with the frequency ω_2 (Figure 21c). As a result of this effect, vectors 1' and 2' are no longer oriented along the -y direction thus the intensity of the echo is reduced.

The orientation of the vector depends on τ , therefore, the maximum contribution is obtained only if during the refocussing process in time τ , precesses an integral number of times, where $2\pi n = (\omega_1 - \omega_2)\tau$. The decay time in the 2-pulse experiment is determined by T_M (or T_2) which is often short, thus the echo and the modulations will decay quickly, resulting in broad lines in the frequency domain.

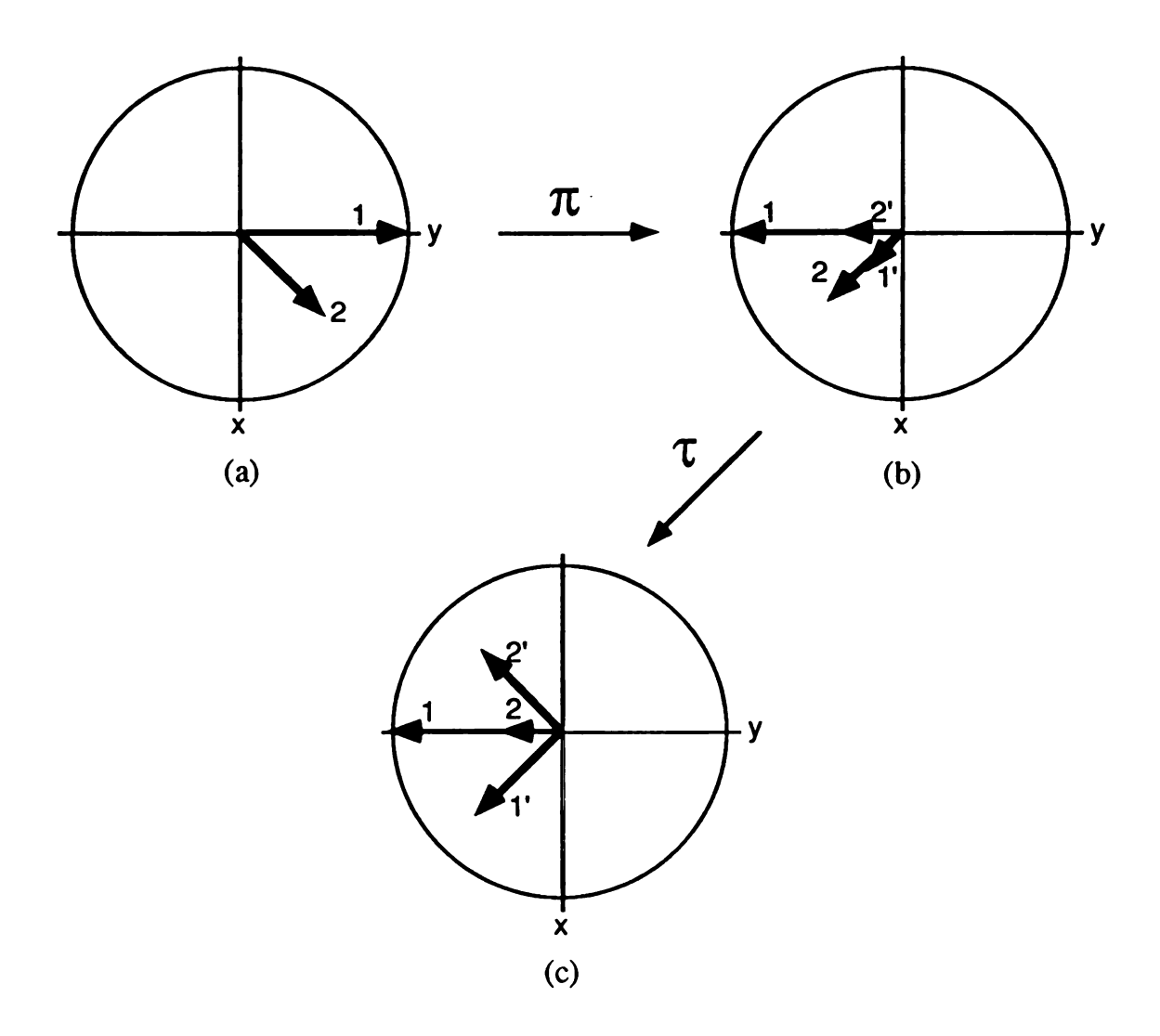


Figure 21: Echo diagram describing echo nuclear modulation a) after $\pi/2$ pulse, b) after π pulse and evolution c) at the time of the echo.

II. EPR Studies of the Photoexcited Triplet States of K+(C222)e- and K+(C222)K-

For over one hundred years, it has been known that many organic compounds could be photoexcited to exhibit a strong phosphorescence or afterglow. However, it was not until the year 1958 that these photoexcited molecules were observed via EPR methods²². The electrons in an S=1 state (triplet) interact with one another to produce markedly different spectra from typical doublet spectra. Here I propose to photoexcite the compounds $K^+(C222)e^-$ and $K^+(C222)K^-$ into their triplet states, and study their EPR properties.

Many properties of alkalides and electrides have been studied, but there has never been direct evidence of the triplet state. Optical spectra of thin films of K⁺(C222)e⁻, showed dramatically different spectra than typical electrides²³. A continually rising absorbance in the near IR region was observed, which is similar to the spectra of metallic solutions of alkali metals in liquid ammonia²³. These results showed that either shallow traps existed, or electron delocalization. Direct current powder conductivity measurements showed an activation energy of about 0.02 eV²³ over a temperature range of 103K - 153K. This result suggested that the compound is not metallic, but instead, that weakly bound electrons exist.

The magnetic susceptibility results showed that this compound consisted mainly of paired electrons as the temperature approached 0 K. As the temperature was increased, the susceptibility increased, suggesting that there was electron pair dissociation, which was thermally induced, or that a triplet state was being populated. This observation will be contemplated by EPR studies.

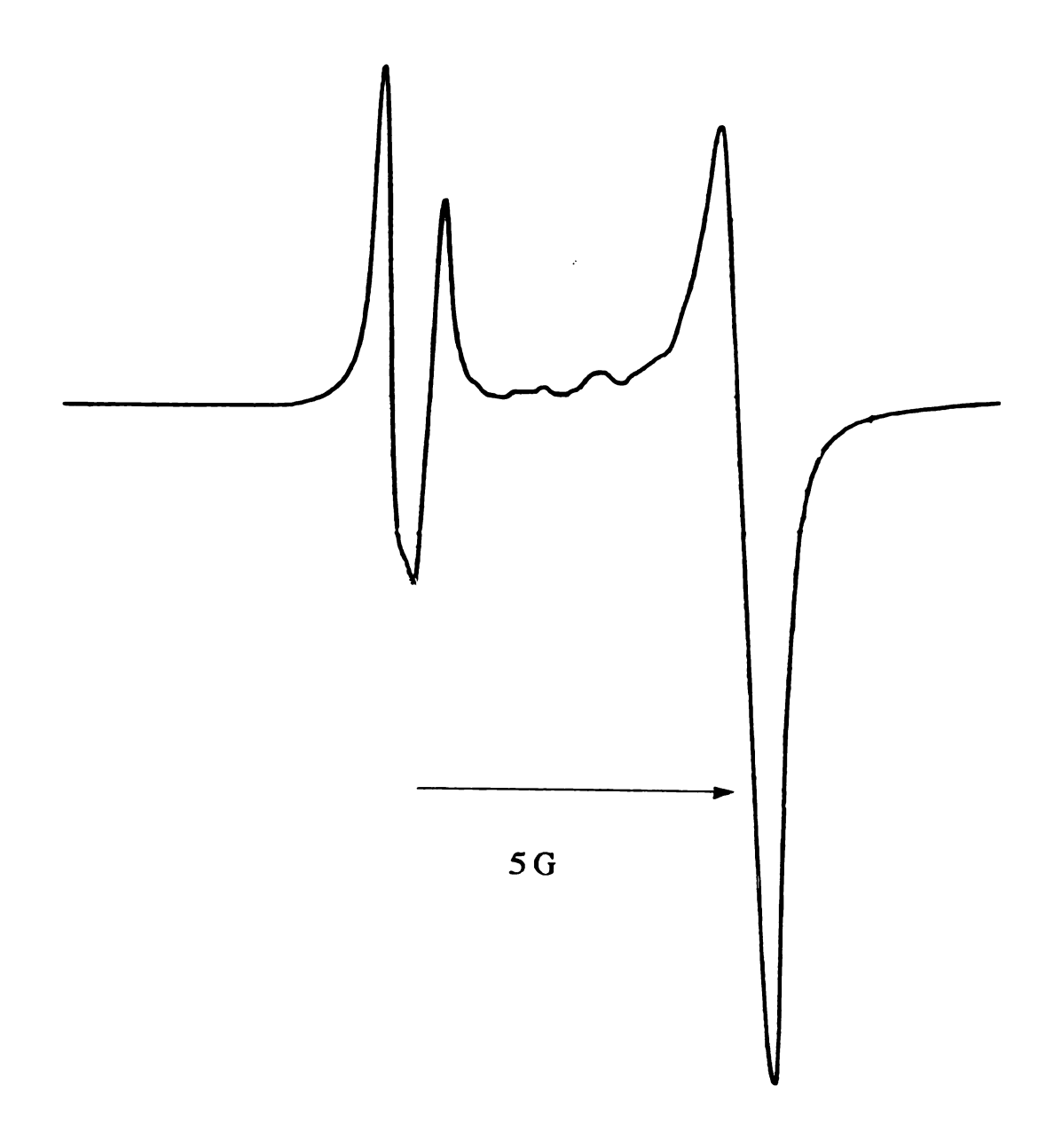
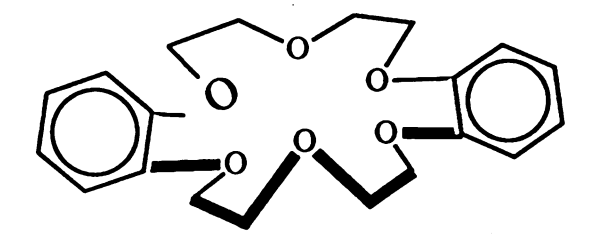


Figure 22: CW-EPR spectrum of K+(C222)K- at 130K

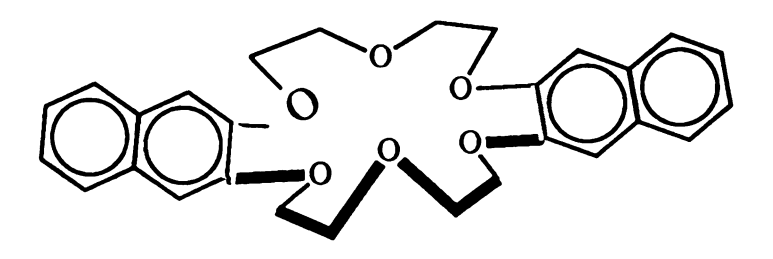
Preliminary EPR results show that the K+(C222)K- compound has axial symmetry (Figure 22). Thus far, attempts have been made to photoexcite these samples with an 800 W projection lamp as well as a UV lamp, but no spectrum indicative of a triplet state has been observed. Both of these compounds have singlet ground states, but it is predicted that they have low lying triplet states, thus different light sources will be used to attempt to observe the triplet state via EPR.

III. Synthesis and Characterization of New Alkalides and Electrides

With such diversities of the properties of the class of compounds discussed thus far, we are anxious to prepare new electrides and alkalides. One of the goals, is to prepare compounds in which the complexant has attached to it, an aromatic molecule, such as benzene or naphthalene (Figure 23). It is of interest to know where the electron will reside in a situation where there is an excess of electrons. Will the electron delocalize into the aromatic molecule or will it remain outside of the complexant completely? Recently, attempts were made to reduce the dibenzo-18C6 (DBC) complexant with both K metal and Na metal. The synthesis was virtually the same as previously described. Solution EPR studies revealed no signal at all, probably due to the fact that benzene is difficult to reduce. In fact, Na is not a strong enough reducing agent to reduce benzene, even in the presence of a complexant. Naphthalene is however much easier to reduce, and we recently acquired some of the dinaphtho-18C6 complexant. This compound will probably serve as a much better model for these types of studies. We plan to focus on the synthesis and study of alkalides and electrides that are expected to exhibit new types of behavior.



Dibenzo-18-Crown-6



Dinaphtho-18-Crown-6

Figure 23: Two aromatic complexants used to produce potential electrides and alkalides.

REFERENCES

- a. Dye, J. L., DeBacker, M. G., Annu. Rev. Phys. Chem. 1987, 38, 271.
 - b. DeBacker, M. G., Sauvage, F. X., Dye, J. L., Chem. Phys Lett., 1990, 73, 291.
 - c. Dye, J.L., Science, 1990, 247, 663.
 - d. Tehan, F. J., Barnett, B. L., Dye, J. L., J. Am. Chem. Soc. 1974, 96, 7203.
- 2. Kraus, C. A., . Am. Chem. Soc. 1974, 96, 7203; Thompson, J. C., Electrons in Liquid Ammonia (Oxford Univ. Press, Oxford, 1976).
- 3. Pederson, C. J., J. Am. Chem. Soc. 1967, 89, 2495, J. Am. Chem. Soc. 1967, 89, 7017, J. Am. Chem. Soc. 1970, 92, 386.
- Lehn, J-M., Sauvage, J. P., Dietrich, B., Tett. Letters, 1969, 1969,
 2885; Tett. Letters, 1969, 1969, 2889; Lehn, J-M., Acc. Chem. Res.
 1978, 11, 49; Lehn, J-M, Angew. Chem. Int. Ed. Engl. 1988, 27,
 89.
- 5. Kittel, C., Introduction to Solid State Physics, John Wiley and Sons, New York, 1986.
- 6. Shin, D-H, Ellaboudy, A. S., Dye, J. L., DeBacker, M. G., J. Phys. Chem. 1991, 95, 7085.
- 7. Ward, D. L., Huang, R. H., Kuchenmeister, M. E., Dye, J. L., Acta. Cryst. 1990, C46, 1831.
- 8. Dawes, S. B., Eglin, J. L., Moeggenborg, K. J., Kim, J., Dye, J. L., J. Am. Chem. Soc. 1991, 113, 1605.

- 9. Moeggenborg, K. J., Papaioannou, J., Dye, J. L., Chem. Of Mat. 1991, 3, 514.
- 10. Dawes, S. B., Ph.D. Dissertation, Michigan State University, 198 6.
- 11. Ward, D. L., Huang, R. H., Dawes, S. B., Dye, J. L., J. Am. Chem. Soc. 1986, 108, 3534.
- 12. Issa, D., Ellaboudy, A. S., Janakiraman, R., Dye, J. L., J. Phys, Chem.
- 13. Dawes, S. B., Ellaboudy, A. S., Dye, J. L., J. Am. Chem. Soc. 1987, 109, 3508.
- 14. Shin, D-H., Ph.D. Dissertation, Michigan State University, 1896.
- a.Landers, J. S., Dye, J. L., Stacy, A., Sienko, M. J., J. Phys. Chem.
 1981, 85, 1096. b. Huang, R. H., Faber, M. K., Ward, D. L., Dye,
 J. L., unpublished results from this laboratory.
- 16. Cauliez, P., Jackson, J. E., Dye, J. L., *Tett. Letters*, **1991**, *32*, 38, 5039.
- 17. For a general treatment of EPR theory, see: a. Wertz, J. E., Bolton, J. R., Electron Spin Resonance Elementary Theory and Practical Applications, McGraw-Hill, New York, 1972. b. Davis, J. C., Advanced Physical Chemistry, The Ronald Press Co., New York, 1965.
- 18. Dyson, F. J., *Phys. Rev.*, **1955**, 98, 2, 349.
- 19. Webb, R. H., Phys. Rev., 1967, 158, 2, 225.
- For a general treatment of pulsed EPR methods, see: a. Schweiger, A., Angew. Chem. Int. Ed. Engl., 1991, 30, 265. b. Keijers, C. P., Reijerse, E. J., Schmidt, J., Pulsed EPR: A New Field of Applications. New York, 1989.

- a. Ellaboudy, A. S., Bender, C. J., Kim, J., Shin, D-H,.,
 Kuchenmeister, M. E., Babcock, G. T., Dye, J. L., J. Am. Chem. Soc.
 1991, 113, 2347. b. Kuchenmeister, M. E., Dye, J. L., J. Am.
 Chem. Soc. 1989, 111, 935.
- 22. Hutchinson, C. A., Mangum, B. W., J. Chem. Phys., 1961, 34, 908.
- Huang, R. H., Faber, M. K., Moeggenborg, K. J., Ward, D. L., Dye,
 J. L., Nature, 1988, 331, 599.

Appendix

Quantization of Angular Momentum

Imagine a particle with mass, m, and a linear momentum described by Eq. 1, with a velocity, v.

$$p = mv (1)$$

If it is assumed that the particle is a quantum mechanical particle, it will have De Broglie wavelength associated with it, as described by Eq. 2,

$$\lambda = h/p \tag{2}$$

The probability of finding a particle at any point in a line, box, ring, etc. is the square of the amplitude of this wave, λ. For the probability to be independent of time, the wave function must maintain a single value. Therefore, there should be no interferences of the wave with itself while traveling around the line, ring, etc. A ring for example, is required to have a circumference which is an integral number of De Broglie wavelengths, M, thus rearranging Eq. 2, and subsequent substitutions results in Eqs. 3-5,

$$2\pi r = M\lambda \tag{3}$$

$$2\pi r = Mh/p \tag{4}$$

$$pr = Mh/2\pi = M\hbar = p_{\Phi}$$
 (5)

The magnitude of angular momentum of the particle is p_{ϕ} , and should be an integral multiple of \hbar where M will also be an integer 0,1,2,...,M = 0 represents an electron in an orbital with no nodes, such as a σ orbital, and M = 1 is the case of an electron in a π orbital. This basic model can be directly applied to the angular momentum of an electron. It is also important to note that the particle in the box, ring etc. represents quantization of angular momentum.

Relating Angular Momentum with Magnetic Moment

Consider the same particle with with mass m, velocity v, charge q, in a circle with radius r. Associated with the current i, is a magnetic field. Associated with that magnetic field is a point dipole with a magnetic moment , μ_z .

$$\mu_{z} = iA \tag{6}$$

where A is the area of a circle, πr^2 and $i = qv/c2\pi r$. Substituting the values for A and i, Eq. 7,

$$\mu_z = qv\pi r^2/c2\pi r = qvr/2c \tag{7}$$

but recall that p = mv from Eq. 1. Substitute this into Eq. 7,

$$\mu_{z} = qmvr/2mc \tag{8}$$

Now substitute p_{ϕ} for mvr to obtain Eq. 9,

$$\mu_z = qp_{\phi}/2mc$$
 (9)

Now let $\gamma = q/2mc$ and substitute this into Eq. 9,

$$\mu_{z} = \gamma p_{\phi} \tag{10}$$

and finally, use Eq. 5 to substitute for p_{ϕ} ,

$$\mu_{z} = \gamma M \, \hbar \tag{11}$$

To convert angular momentum to the magnetic moment, use Eq. 12,

$$q = -e/2mc (12)$$

but in general,

$$\gamma = -ge/2mc \tag{13}$$

where g is a factor that must be included for all cases, except a system with purely orbital angular momentum. For every multiple of orbital angular momentum, there is an orbital magnetic moment of eh/ 4π mc. In the case of an electron, this whole expression is simplified as β or the Bohr magneton (β = 9.2741 x 10⁻²¹ erg/G). For electron spin, the value of g is 2.00232 (for a free electron, g_e). So μ_z can now be written with respect to the magnetic field, H, as (Eq. 14)

$$\mu_{z} = \gamma M_{s} \, \hbar \tag{14}$$

where M_s is the spin quantum number. Re-writing this expression while substituting $\beta g/\hbar$ for γ yields Eq. 15,

$$\mu_{z} = g\beta M_{s} \tag{15}$$

Quantization of spin angular momentum leads to quantization of energy levels. From before, $E = -\mu_z H$ and substituting Eq. 15 for μ_z ,

$$E = g\beta M_s H \tag{16}$$

Many transitions can be drawn in an energy level diagram and comparison with the observed spectrum shows that not all transitions occur. Thus there is a notion of "allowed" and "forbidden" transitions. "Allowed" transitions require a knowledge of the EPR selection rules. When the energy of a quantum (monochromatic incident radiation) matches the energy level separation, absorption occurs. The selection rule, $\Delta M_s = \pm 1$ leads to possible values of $M_s \pm 1/2$. This leads to values of energy (Eq. 17),

$$E = \pm 1/2g\beta H \tag{17}$$

and these energies are referred to as the Zeeman energies.

